QUALITATIVE HPLC ANALYSIS OF PEPTIDE FUNCTIONALIZED FLUORESCENT SILICA-NANOPARTICLES FOR APPLICATIONS IN NANOMEDICINE

A Thesis

Presented to the Faculty of the Graduate School

Of Cornell University

In Partial Fulfillment of the Requirements for the Degree of

Master of Science

By

Shaun Javier Alvarado

January 2017

© 2017 Shaun Javier Alvarado

ABSTRACT

Functionalized nanoparticles are widely used for various medical applications, defined as nanomedicine. Notwithstanding, surface functionalization remains poorly understood. Distributions of surface ligands per particle are rarely considered or measured for the appropriate methods are lacking. This research aims to establish a procedure for qualitatively analyzing said distributions. The nanostructures of interest are peptide, and polyethylene glycol (PEG) functionalized fluorescent silica nanoparticles, Cornell Prime dots (C' dots). Average surface ligands per particle were measured as shown in previous work.[1,2] Then these C' dots were fractionated by size with Gel Permeation Chromatography (GPC) and separated by surface chemistry with High Performance Liquid Chromatography (HPLC). Peptide distributions per particle were indiscernible from PEG; this finding indicates that PEG functionalization is not as homogenous as previously considered, and contributes significantly to surface heterogeneity. Additionally, despite uncoupling the contributions of functionalized particle sizes, results indicated size had little impact on surface ligands per particle distributions.

BIOGRAPHICAL SKETCH

Shaun Alvarado is a Tampa Bay area native Floridian, of Puerto Rican parentage. He earned his A.A. in Engineering at Hillsborough Community College, and his B.S. in Chemical Engineering from the University of Florida.

I dedicate this thesis to my lovely wife and soulmate, Estefanía Alvarado, thank you for your love, admiration, and support; *Te amo y te quiero mi amor, con toda mi alma.*

TABLE OF CONTENTS

LIST OF FIGURES

LIST OF TABLES

INTRODUCTION

Nanomedicine is an emergent field of medical science that amalgamates medicine with materials science, nanoscience, pharmaceutics, immunology, molecular biology, and clinical translational research. The aim of this work is to study and exploit unique material properties in nanomaterials, along with physical, chemical, and biological phenomena. The advancement of nanomedicine is professed to prevent disease and traumatic injury, relieve pain, and to build up the domains of medical diagnosis and therapy in the form of theranostics, a recent therapeutic paradigm in the approach to pathology.[3] The aim of the field of nanomedicine, as summarized by the European Science Foundation, is to enhance human health through the monitoring and controlling of human biological systems with engineered devices and nanostructures.[2] Nano-devices and structures are by definition limited by size, on at least one dimension of hundreds of nanometers to a single nanometer, with a focus on nano-interactions affecting larger systems such as tissues or intracellular processes.[2]

Fluorescent nanoparticles, a type of nanostructure that has three dimensions on the nanoscale, and their applications for targeted diagnostics and therapeutics in nanomedicine have made great strides in recent years.[2,4] For appropriate transport to specific cell types for imaging or drug delivery, nanoparticles must be functionalized with targeting ligands or peptides. Currently, nanoparticle fabrication relies on a series of batch syntheses and filtration steps to capture desired size distributions. Controlling the distribution of ligands per particle, is challenging using batch synthesis; due to limited control over mixing efficiencies resulting in heterogeneous reagent concentrations throughout the bulk solution.[5]

In the fields of nanomedicine and ligand-nanoparticle materials, the functionalization of nanoparticles with surface targeting ligands is often un-quantified and reported as the average ligand ratio, if reported at all, whether for biocompatibility, targeting, drug delivery, or imaging. Ligands per particle averages provide insufficient data regarding the heterogeneity and distribution of targeting ligands.[6] The average number of ligands per particle inadequately characterizes these materials; in fact, ligand distributions vary significantly from sample to sample.[7] Unfortunately, the impact of targeting ligand densities and distributions on targeted cell binding efficiency and biological response remains poorly understood.[7,8]

Measurement of targeting ligand distributions could significantly improve understanding of nanoparticle synthesis and behavior for theranostic, diagnostic and therapeutic, applications.[7] Further, the ascertainment of the distribution of ligands would fundamentally transform how these materials are characterized and optimized for targeting, solubility, and stability.

This unfortunate lack of understanding and data for optimization is a direct consequence of existing analytical techniques' inability to measure targeting ligand distributions. Current techniques include: Fourier transformed infrared spectroscopy (FTIR), nuclear magnetic resonance (NMR), matrix-assisted laser desorption ionization time-of-flight (MALDI-TOF), and ultraviolet/visible (UV/vis) spectroscopy.[6] The failure to quantify targeting ligand distributions is a major limitation for the optimization of nanomedicine nanoparticles; distributions may vary significantly even when averages of ligands per particle between samples are equivalent. This limitation adds yet another convolution to an already exceedingly complex biological system when nanoparticles are used for diagnostic or therapeutic applications. The intricacy is in part due to the heterogeneity of the targeting ligands per nanoparticle and its possible effects on targeting efficiency, pharmacokinetics profiles, and nanoparticle biodistribution. However, if nanoparticles could be synthesized with enhanced homogeneity from an understanding of the targeting ligand distribution quantification, a more simplified approach to study these particles for diagnostics and therapeutics would be possible.

High-Performance Liquid Chromatography (HPLC) may be employed to measure quantitatively surface targeting ligands per particle distributions. Utilizing HPLC to characterize ligands per nanoparticles has yet to be explored. It is suspected that this type of technique may be employed from the data presented by Mullen *et al.* of poly(amidoamine) (PAMAM) dendrimer measurements via HPLC.[7] Distributions of surface ligands per particle were not appropriately described by a single Gaussian distribution, but a distribution of multiple Gaussian distributions. Additionally, findings indicated that average surface ligands per particle measurements do not accurately represent particle surface functionalization on the majority of particles in a given sample.[6,7]

The nanomedicine nanoparticles of scope and concern are C Dots, developed by Ow *et al*.[9,10] C Dots are amorphous organo-silica fluorescent nanoparticles synthesized in ethanol, with tunable diameters ranging

from sub-10 to 30 nm; these particles are more photostable and 20 times brighter, than constituent dyes.[9,10] The development was based on a modified Stöber process, an alcoholic synthesis of silica particles derived from silica sol-gel chemistry yielding particle sizes ranging from 50 nm to 2 μm.[9–11] Sub-10nm C Dots exhibited promise as clinically relevant nanoparticles due to the biocompatibility of amorphous silica and that sub-10 nm, or ultrasmall, particles will rapidly clear from the body via renal clearance pathways.[12–14] These ultrasmall C Dots were used for cancer imaging as the first-in-human nanoparticle diagnostic of its kind, with clinical trials conducted at the Memorial Sloan Kettering Cancer Center (MSKCC).[2,12,15]

In 2015, a water-based synthesis of sub-10 nm silica nanoparticles (known as Cornell Prime Dots or C' Dots to distinguish water-based from the ethanol-based syntheses) were developed by Ma *et. al.*; the water-based synthesis simplifies purification for clinical applications substantially.[16] Both C Dots and C' Dots can be synthesized with fluorescent or near-infrared (NIR) fluorescent dye molecules in a silica core, functionalized with polyethylene glycol (PEG), targeting ligands and radio isotopes (for positron emission tomography (PET) imaging)[16,17]. Another important feature of C Dots and C' Dots is their ability to covalently bind PEG to the nanoparticle surface, known as covalent PEGylation. This enables the nanoparticles to exhibit improved pharmacokinetic profiles and biodistribution.[18] Figure 1 presents a schematic of the C Dots used in the study of Human Melanoma patients.[2]

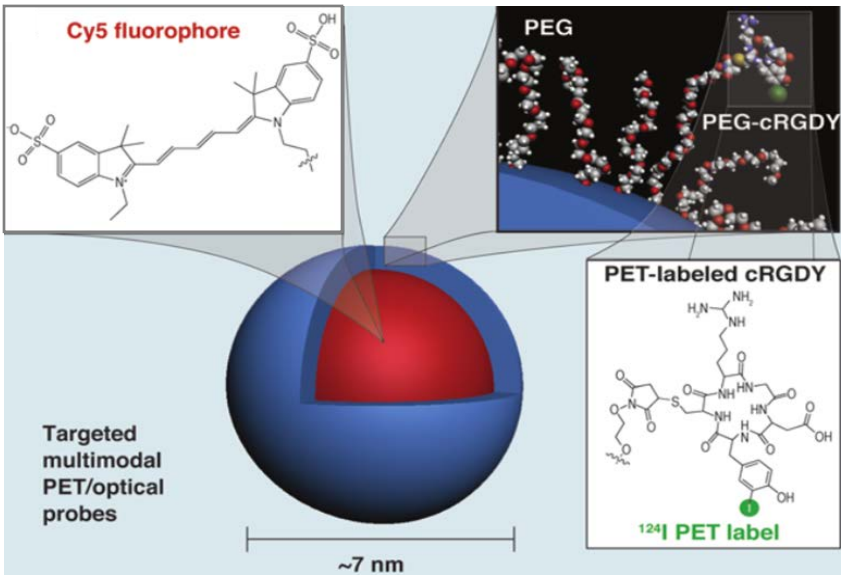

Figure 1: Schematic representation of C Dot structure with Cy5 fluorophore, surface functionalized with PEG, PEG-cyclic (arginine, glycine, aspartic acid, D-tyrosine-cysteine) (cRGDY) targeting ligands, and labeled with iodine-124 for PET imaging.[2]

EXPERIMENTAL SECTION

MATERIALS

Chemicals were used as received without further purification. 2M ammonium hydroxide in ethanol, 3-aminopropyl) triethoxysilane (APTES), tetramethyl orthosilicate (TMOS), dimethyl sulfoxide (DMSO), and silicon oil were purchased from Sigma Aldrich. HPLC/UPLC grade 2-propanol was purchased from J.T. Baker. HPLC/UPLC grade methanol and acetonitrile were purchased from VWR Analytical. Methoxy-silane terminated poly (ethylene glycol) chains (PEG-silane, molecular mass approximately 500 g/mol) and 3-mercaptopropyl trimethoxysilane (MPTMS) were purchased from Gelest. Maleimide-dPEG®12-NHS ester (bi-functional PEG, molecular mass 865.92 g/mol) was purchased from Quanta Biodesign. The peptide, cyclo (arginine-glycine-aspartic acid, D-tyrosine-cysteine) (cRGDY molecular mass 594.65 g/mol), was purchased from Peptides International. Cy5 maleimide functionalized fluorescent dye, Vivaspin® 500 protein concentrator (MWCO 30K spin-filter), and Superdex 200 Prep Grade chromatography resin were purchased from GE Healthcare Life Sciences. 5M sodium chloride solution was purchased from Chem Cruz. SnakeSkin™; dialysis tubing (10K MWCO) was purchased from Thermo-Fisher Scientific. Polyvinylidene fluoride 0.22 µm syringe-filter unit was purchased from Millex-GV. The 35 mm No. 1.5 micro-well dish used for fluorescence correlation spectroscopy was purchased from MatTek Corp. Deionized water was obtained from a Millipore Milli-Q system.

SYNTHESIS

Synthesis of C' dots functionalized with Cy5 dye and cRGDY peptide, to make cRGDY C' dots, was performed by following procedures developed by Ma *et. al*.[1,2] Two separate batches of cRGDY C' dots were synthesized; the first sample (120 µL cRGDY C' dots) was functionalized with 120 µL of cRGDY the second sample (60 µL cRGDY C' dots) was functionalized with 60 µL of cRGDY. The final concentration of cRGDY for each sample was 2.5 nM and 1.3 nM for the 120 µL and 60 µL cRGDY C' dot samples, respectively. All other experimental conditions were identical between each sample. The synthesis was segmented in three major phases, cRGDY conjugation with PEG-silane, Cy5 conjugation to a silane, and sub-10nm silica nanoparticle (C' dot) synthesis using the conjugated Cy5 and cRGDY moieties.

cRGDY conjugation

Before the conjugation of cRGDY with the silica surface, the cRGDY must be labeled with a PEG-silane group to facilitate cRGDY condensation with the C' dot silica surface.[2] Within an MBraun® glove box in nitrogen environment, one day prior to cRGDY conjugation, DMSO was added into the stock bottle of cRGDY to solubilize and yield a solution of concentration of 0.0125 mg cRGDY/mL DMSO (~21 µM). The solution was micropipette mixed 100 times with a 100 µL or 1000 µL pipette set to at most half of the amount of DMSO added to the cRGDY stock vessel. The term "micropipette mix" refers to the act of slowly siphoning a mixture up to the target volume, and back down in to the storage vessel. DMSO was added to a stock solution of bi-functional PEG such that the concentration of 200 mg/mL bi-functional PEG to DMSO was obtained and micropipette mixed 100 times. A micro stir bar (1.5 mm or 3 mm in diameter and length) was added to each stock bottle (cRGDY and bi-functional PEG), and stirred at 200 RPM overnight. 40 µL of DMSO and 10 µL of APTES were added to a 1.5 mL micro-tube, labeled "APTES" with 100 µL and 10 µL micropipettes, respectively. The APTES/DMSO solution was micropipette mixed 50 times with a 100 µL micropipette set to 40 µL. Separately, 12 µL of DMSO and 12 µL bi-functional PEG were added to a 1.5 mL micro-tube labeled "MPS", with a 100 µL micropipette and micropipette mixed 50 times. The MPS abbreviation denotes the Maleimide-PEG-Silane product that resulted from a reaction between APTES and bi-functional PEG. 2.92 µL of the APTES/DMSO from the micro-tube labeled "APTES" was added to the

micro-tube labeled “MPS” with a 10 µL micropipette, and micropipette mixed 100 times with a 100 µL micropipette set to 12 µL. The MPS solution was left at ambient temperature in the glove box for two days. After a period of two days, a 100 µL micropipette was set to 60 µL and 120 µL cRGDY/DMSO was added to a micro-tube labeled “RGD”. Additionally, 22.2 µL of MPS or silane-labeled bio-functional PEG from the micro-tube labeled “MPS” was added to the micro-tube labeled “RGD” with a 100 µL micropipette and was micropipette mixed 100 times with a 100 µL micropipette set to 60 µL. For the sample that consisted of half the original amount of cRGDY, 60 µL of cRGDY and 11.1 µL of MPS were used. The cRGDY/MPS solution was kept at ambient temperature within the glove box overnight.

Cy5 dye conjugation

In order to be able to conjugate covalently a dye to the silica particle core, the dye was functionalized with a silane group. To that end, within a glove box under nitrogen, stock Cy5 with a pending maleimide group was dissolved in DMSO to a concentration of 50 mg/mL and micropipette mixed 100 times, with a micropipette that was set to at most half the total volume of DMSO added. The solution was kept in the glove box at ambient temperature overnight. After the first day of cRGDY conjugation, with a 100 µL micropipette, 94 µL of DMSO and with a 10 µL micropipette, 6 µL of Cy5/DMOS were added to a 1.5 mL micro-tube, labeled “Cy5”. The solution was then micropipette mixed 50 times with a 100 µL micropipette set to 50 µL. 1.58 µL of MPTMS was added with a 10 µL micropipette to the micro-tube labeled “Cy5”, and micropipette mixed 50 times with a 100 µL pipette set to 50 µL. The Cy5/MPTMS solution was kept in the glove box at ambient temperature overnight.

Sub-10 nm silica nanoparticle synthesis

A 0.2 mM solution of 2 M ammonia was first prepared in ethanol. 10 mL of deionized water was added, with a 10 mL tip in an auto-pipette, to a 20 mL glass tube, which was rinsed 10 times with deionized water, dried with compressed air, and labeled “dilute ammonium hydroxide”. With a 100 µL micropipette, 100 µL of 2 M ammonia in ethanol was added to the dilute ammonia solution, and mixed with a vortex mixer set to 8 for 10 seconds. Separately, a 25 mL round bottom flask, 16 mm egg-shaped magnetic stir bar, and a rubber stopper were washed and rinsed with Alconox® glassware cleaner and water. Each item was then rinsed

in deionized water 10 times and dried with compressed air. The magnetic stir bar was placed in the flask, and with a 10 mL tip auto pipette, 9 mL of deionized water was added to the flask. The flask was then set on a cork stand within a chemical fume hood on a stir-plate set to 600 RPM, or at a stir rate sufficient to allow a vortex to form on the magnetic stir bar. 1mL of dilute ammonia solution was added to the flask with a 1000 µL micropipette; drop-wise additions were placed on the inner edge of the vortex. The rubber stopper was placed on the flask, and the solution was stirred at ambient temperature for 5-minutes. During the 5-minute wait time, the micro-tube labeled “Cy5” was obtained from the glove box. After the 5-minute wait time, the rubber stopper was removed, and a 100 µL micropipette was used to add 68 µL of TMOS drop wise in the flask, on the inner edge of the vortex. Immediately after TMOS addition, the content of the micro-tube labeled “Cy5” (101.58 µL) was added dropwise to the inner edge of the vortex, with a 200 µL micropipette set to 102 µL. Dropwise in the context of this protocol means adding the fluid very slow and steady, drop by drop. The solution continued to stir at 600 RPM, or adjusted to ensure the vortex and magnetic stir bar meet. A rubber stopper was placed on the flask and the reaction left overnight at ambient temperature. On the subsequent day, the micro-tube labeled “RGD” (cRGDY conjugated to PEG-Silane) was obtained from the glove box, and a 200 µL micropipette, set to 143 µL, was used to move the content of the RGD micro-tube (142.2 µL) dropwise to the flask on the inner edge of the vortex. For the 60-µL cRGDY C’ dot sample, 71.1 µL of cRGDY conjugated to PEG-Silane was added. Immediately after cRGDY addition, with a 100 µL micropipette, 100 µL of PEG-Silane was added to the flask dropwise to the inner edge of the vortex. The flask was sealed with a rubber stopper and the reaction was stirred overnight at ambient temperature. On the following day, the flask was removed from the stir plate and placed into a silicon oil bath over a hot plate, with a beaker stand and clamps to secure the flask to the center of the silicon oil bath. The hot plate was set to 80^{o}C and held overnight. On the consecutive day, the solution was cooled to ambient temperature and transferred stepwise from the flask with a 1000 µL micropipette set to 1000 µL to dialysis tubing secured on one end with a plastic clamp. The dialysis membrane was submerged in 2.0 L of deionized water. Dialysis continued for 2 days, during which the deionized water was changed once each day. After 2 days of dialysis, the solution was transferred from the dialysis membrane to a rinsed and dried 20 mL glass tube and filtered through a 0.22 µm syringe filter. The filtered solution was stored at 8^{o}C for further characterization and purification with Gel Permeation Chromatography.

CHARACTERIZATION

cRGDY surface functionalized C' Dots were characterized utilizing various instruments and techniques as shown by Ma *et al.* (with the exception of HPLC analysis).[1,2,16] To obtain hydrodynamic radius, sample concentration, and average number of dyes per particle, as well as an estimate of the average targeting ligands per particle, fluorescence correlation spectroscopy (FCS) as well as ultraviolet/visible spectroscopy (UV/Vis) were performed, respectively.

Gel Permeation Chromatography (GPC)

Purification of cRGDY C' dots was performed with a Bio-Rad BioLogic™ LP System which consisted of a GPC column with Superdex 200 resin with a 0.9% NaCl aqueous buffer solution (mobile phase) and fraction collection unit. GPC is a form of Size Exclusion Chromatography (SEC), which utilizes a gel or resin, with an average particle size on the order of microns, as a stationary phase that facilitates larger (macro-) molecules to migrate through the gel faster (i.e. with shorter elusion times) than smaller (macro-) molecules. The smaller molecules become entrenched within the porous gel particles, thereby eluting at later times.[19] The resulting difference in elution times between large (macro-) molecules and small (also macro-) molecules enables the separation of cRGDY C' dot particle product from silica aggregates, free dye, and free surface ligands (PEG and cRGDY).

Samples were first concentrated with centrifuge filters at a molecular weight cut-off of 30K Daltons, placed in an Eppendorf centrifuge for 45 minutes at 4270 RPM. The remaining sample, typically 100 µL, was collected and loaded on to the resin, with a mobile phase flow rate of mL/min. Samples were collected with a frequency of 0.3 min per fraction. The GPC utilizes a UV detector (single channel set to 280 nm), which measures the difference in absorbance between the mobile phase and sample. The data is recorded as an increase in absorbance due to the presence of sample versus the elution time from the column.

Figure 2 shows the resulting chromatogram set of the 280 nm wavelength channel of the synthesized cRGDY C' dots. From previous experience the signal peaks can be assigned as follows:[16] C' dots signal appears between elusion times 12–19 minutes with a peak maximum centered around 15 minutes; A particle aggregation peak appears at earlier elusion times of 8–11 minutes. Finally, free dye appears at

later elusion times (between 20-23 minutes), due to being significantly smaller than the particles. Fractions between 13–18 minutes were collected in order to separate cRGDY particles from aggregates and free dye, and were transferred to a centrifuge filter and spun for 45 minutes at 4270 RPM. The remaining solution after centrifugation is then manually loaded onto the GPC column and run again.

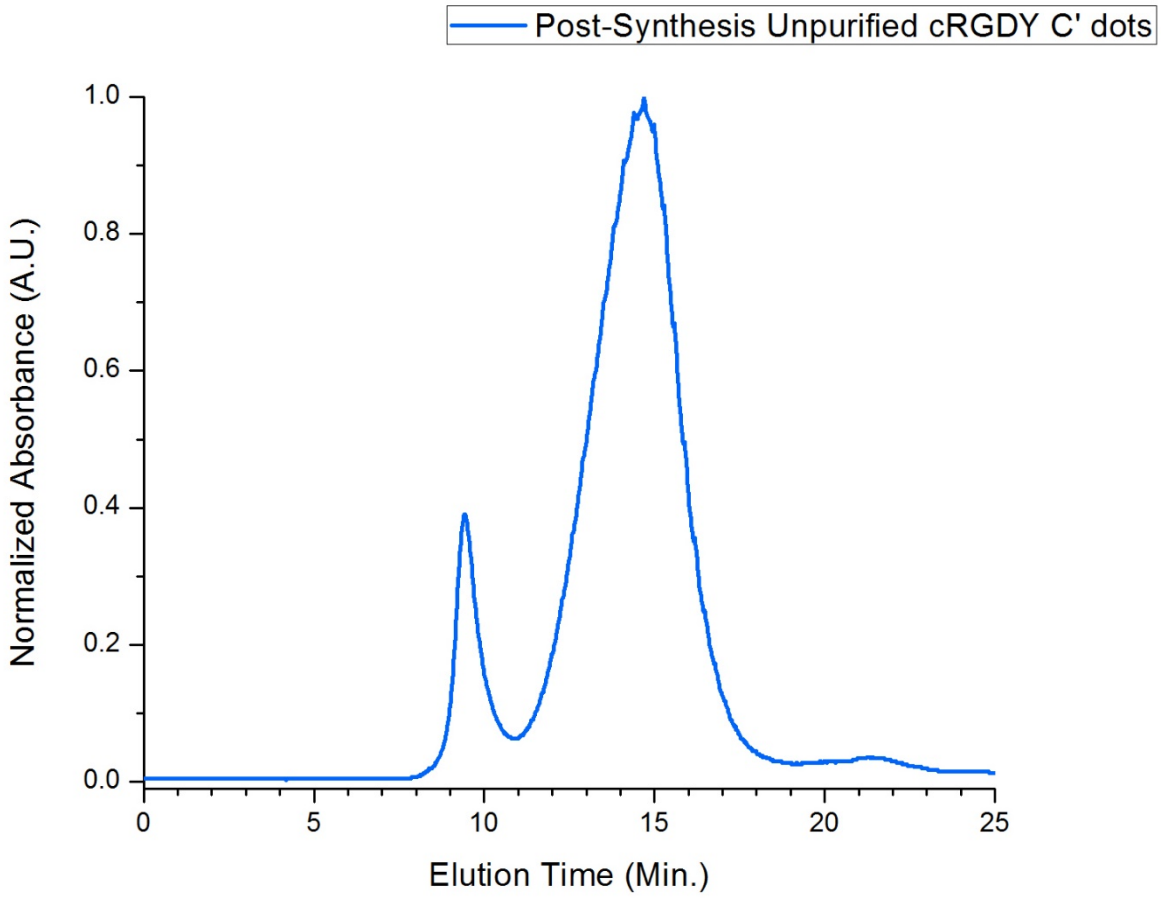

Figure 2: Representative post-synthesis GPC chromatogram of cRGDY C' dots

Iterations of this GPC purification continue until no traces of aggregates and free dye are observed. Figure 3 shows the resulting chromatogram of the GPC purified sample of pure cRGDY C' dots. The elugram in Figure 3 clearly misses peaks of both aggregates and free dye. Additionally, the skewness seen in Figure 2 for the main peak is significantly reduced; however, a slight skewness is still observable. The skewness may indicate the presence of sub-populations of particles, possibly due to size differences or from varying surface ligand densities and numbers of ligands per particle. These effects are further investigated with HPLC in later sections.

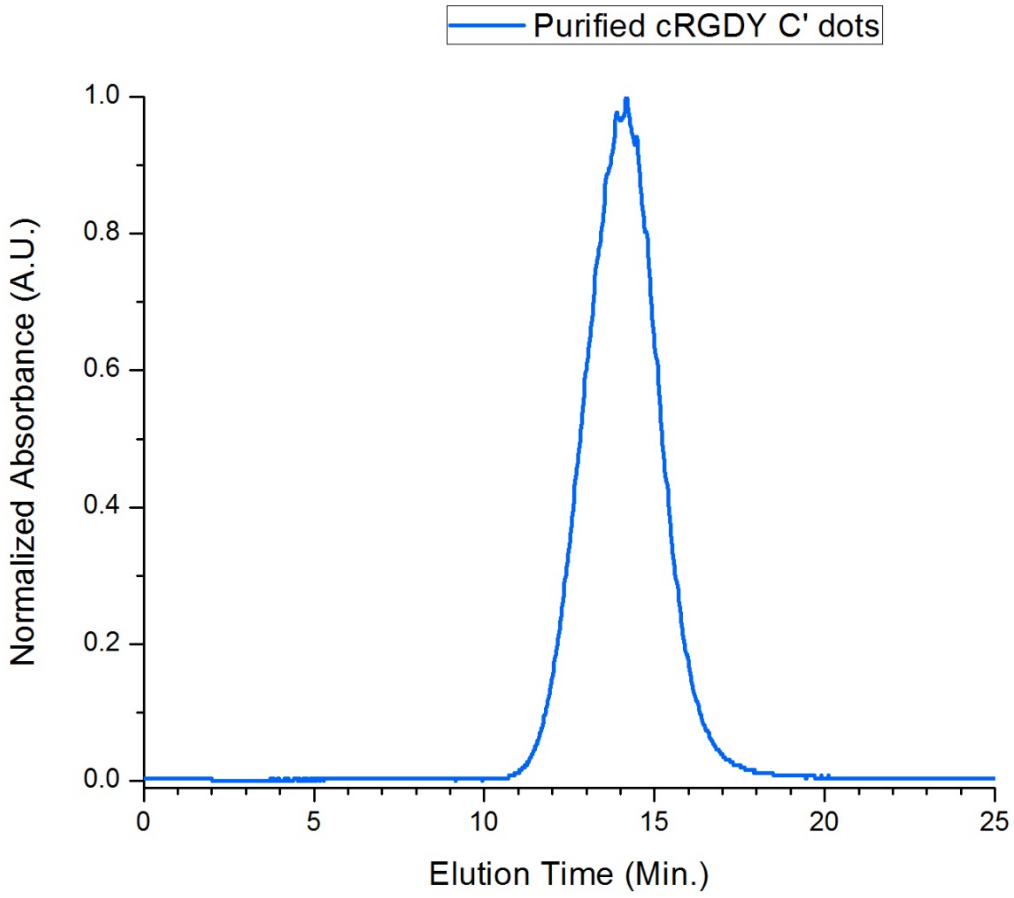

Figure 3: GPC chromatogram of purified cRGDY C' dots

Fluorescence Correlation Spectrometry (FCS)

FCS measurements were conducted on a home-build set-up, further detailed by Herz et al., consisting of a 635 nm solid state laser and a Perkin Elmer avalanche photodiode detector.[20] Essentially, the detector measures the fluctuation in fluorescence intensity (counts) emitted by a given sample as it diffuses through the focal volume of a microscope objective. For homogenous samples, fluorescence intensity count ensemble averages are constant, equivalent and the time average may be represented by Equation 1.[21] Here $F(t)$ represents the fluorescence intensity ensemble average from the start of a measurement, t=0, to the end of the measurement, t=t*.

Equation 1

$$\langle F \rangle = \lim_{t^* \to \infty} \left[\int_0^{t^*} dt F(t) \right]$$

Equation 2 defines the fluorescence intensity fluctuations as $\partial \mathrm{F(t)}$, of $F(t)$ from $\langle \mathrm{F} \rangle$.[21]

Equation 2

$$\partial F(t) = F\ (t) - \langle F \rangle$$

The correlation of fluorescence fluctuations at later time t + τ generates the first order fluorescence fluctuation autocorrelation function. Normalizing the first order autocorrelation function with the fluorescence intensity ensemble average squared, results in the temporal autocorrelation fit function for a three-dimensional, one-component diffusion in a prelate Gaussian focal volume $\mathrm{G}(\tau)$, Equation 3, and the analytical form, Equation 4.[21,22] In Equation 4, N is the number of species diffusing in the focal volume, D is the diffusion coefficient of the diffusing species (here C' Dots), τ is the incremental time during which fluctuations in fluorescence intensity occur, and w_{xy} and w_z are the horizontal (short) and axial (long) distances within the focal volume, respectively.

Equation 3

$$G(\tau) = \frac{\langle \partial F(t)\, \partial F(t+\tau) \rangle}{\langle F \rangle^2}$$

Equation 4

$$G(\tau) = 1 + \frac{1}{N}\left(1 + \frac{4D\tau}{w_{xy}^2}\right)^{-1}\left(1 + \frac{4D\tau}{w_z^2}\right)^{-1/2}$$

Alternatively, Equation 7 is a simplified version introducing diffusion time, τ_D, and structure factor, S, from relations shown in Equation 5 and Equation 6.

Equation 5

$$\tau_D = \frac{w_{xy}^2}{4D}$$

Equation 6

$$S = \frac{w_{xy}}{w_z}$$

Equation 7

$$G(\tau) = 1 + \frac{1}{N}\left(1 + \frac{\tau}{\tau_D}\right)^{-1}\left(1 + \frac{\tau S^2}{\tau_D}\right)^{-\frac{1}{2}}$$

The simplified fit function enables the structure factor (the ratio of the horizontal and axial distances within the focal volume) to be estimated from measurement of a species with known concentration and diffusion coefficient. For example, by absorption matching Cy5 and cRGDY C' dots to AF647, FCS measurements of AF647 may be performed to obtain a structure factor for the FCS measurement analysis of Cy5 dye and cRGDY C' dot particles.[20] In FCS measurements, a significant contribution to the fluctuations may occur from a dye that undergoes high amounts of excitations into the triplet state. Triplet state excitations of dyes result in observable on/off events, or blinking, while in the focal volume, rather than a single emission event from excitation and decay to the ground state. Such blinking events cause inconsistencies in the fluorescence intensities and increases in the autocorrelation signal at short time scales (i.e. nsec-μsec), thereby increasing measurement error. Adjustments to the fit function to account for triplet state phenomena were made as shown by Schwillie *et al.* and documented in Equation 8.[16,23] Here, τ_R is the theoretical diffusion time of triplet state molecules, and A is the fraction of molecules in the off or dark state due to the triplet state effect.[23]

Equation 8

$$G(\tau) = 1 + \left(\frac{1}{N}\right)\left(\frac{1}{1-A}\right)\left(1 - A + Ae^{\left(-\frac{\tau}{\tau_R}\right)}\right)\left(\frac{1}{1+\frac{\tau}{\tau_D}}\right)\left(\frac{1}{\left(1+\frac{\tau S^2}{\tau_D}\right)^{1/2}}\right)$$

Knowing the diffusion time across the focal volume yields the diffusion coefficient, which is then used to calculate the hydrodynamic radius of e.g. C' Dots from Equation 9, the Stokes-Einstein relation.[24]

Equation 9

$$D = \frac{k_B T}{6\pi\mu R_o}$$

where D is the diffusion coefficient of C' Dots, k_B is Boltzmann's constant, T is ambient temperature, μ is fluid viscosity and R_o is the hydrodynamic radius of C' Dots. Fitting the autocorrelation curve to experimental data the number of diffusing species at time t, $N(t)$, is extracted.[25] $N(t)$ is then used to calculate the number of photon counts per second per C' Dot from Equation 10.[25]

Equation 10

$$F(t) = qN(t)$$

Here, $F(t)$ is the fluorescence intensity per unit time, q is the number of photon counts per second, and $N(t)$ is the number of C' Dots diffusing through the focal volume at time *t*.

Ultraviolet/visible spectrophotometry (UV/Vis)

Absorbance measurements were performed on a Cary 5000 absorbance spectrophotometer. The spectrophotometer emits light ranging from 200 nm to 800 nm wavelength and the detector records the intensity of light as a voltage digitized using computer software.[26] Equation 11 represents absorbance as the logarithmic ratio of the intensity of the light source and the intensity of light that is transmitted through a sample contained in a 3.5 mL quarts cuvette.

Equation 11

$$A = \log\left(\frac{I_0}{I_s}\right)$$

Here, A, is absorbance, I_o, is the intensity of the light source, and I_s, is the intensity of light transmitted through the sample. The sample absorbs photons from the light emission source, allowing only a fraction of the light sent to the sample to transmit through.[27] Since the wavelength at which a given molecule absorbs light is relatively unique, molecular species within the sample may be differentiable. Data is generated from measurements as absorbance versus wavelength.

Before the measurement of cRGDY C' Dots, a reference dye with known diffusion coefficient, molar attenuation coefficient, and with excitation/emission wavelengths similar to the Cy5 dye was used to align the FCS setup. Alexa Fluor® 647 (AF647) was used as a reference dye for FCS measurements, because of decreased sensitivity to photobleaching compared to Cy5 dye and its known diffusion coefficient. A known diffusion coefficient allows for the structure factor (the ratio between the short (w_{xy}) and long (w_z) sides of the elliptical focal area) of the laser used for FCS to be measured.[16] The structure factor is a parameter used in the FCS autocorrelation fit function; see Equations 7 and 8 above.

The Lambert-Beer- law (Equation 12) was used to obtain the concentration of cRGDY C' Dots from the concentration of Cy5 dye.[20]

Equation 12

$$A = \varepsilon c L$$

Here, A is absorbance of dye (or ligand), ε is the molar extinction coefficient, which is wavelength-dependent, c is concentration of sample, and L is the path length. The optical density was matched at the peak absorption at 647 nm with the simplified relation shown in Equation 13 for solutions of cRGDY C' Dots and Cy5 dyes.

Equation 13

$$\frac{A_1}{v_1} = \frac{A_2}{v_2}$$

In Equation 13, A_1 is the absorbance of the reference dye (Cy5 for cRGDY C' dots); v_1 is the volume of reference dye used for absorbance measurements. A_2 is the absorbance of the particle being matched to the reference dye, and v_2 is the total volume, the original volume of particles plus additional volume needed to match the absorbance of the reference dye. A baseline of deionized water was taken before each absorption measurement for each sample.

High-Performance Liquid Chromatography (HPLC)

A Waters® e2695 separations module with 2998 PDA UV- detector, Waters XBridge® Protein BEH C4 Column (3.5 µm, 4.6 x 150 mm) and a solvent (mobile phase) consisting of deionized water (phase A) and acetonitrile (phase B) mixture was used to analyze un-fractionated and GPC fractionated cRGDY C' dot samples. HPLC is a high pressure (generally 13-100 MPa) liquid chromatography technique which utilizes physicochemical interactions between the sample, mobile phase and the column packing known as the stationary phase (porous silica gel functionalized with alkyl groups) to separate sample constituents; the high pressure conditions allow for improved separation and decreased run times.[28] For the analysis of cRGDY C' dots, hydrophobic interactions between the PEG and cRGDY on the surface of the particles with the alkyl group on the stationary phase increase migration of the cRGDY C' dots through the column. Particles with greater cRGDY loading would be retained within the stationary phase for a shorter time span than particles with fewer cRGDY ligands per particle, thereby enabling the characterization of the cRGDY per particle distribution. In conjunction with GPC, the cRGDY C' dot particles are first fractionated by size and then with HPLC further separated based on cRGDY per particle. This experimental protocol enables a simplified approach to study only the surface characteristics independent of particle size. HPLC experiments were run under a reverse-phase mode with a gradient elution. Reverse-phase is a regime in which the stationary phase is non-polar and the mobile phase is polar, and gradient elution refers to concentration changes in the mobile phase.[28] Gradient elution from weak polar mobile phases (i.e. water) to strong polar mobile phases (i.e. acetonitrile) increase solvent strength, balance the adsorption-desorption behavior of macromolecules, and enhance separation.[29] Constituents within the sample are separated in the chromatogram based on the rate of migration through the stationary phase and are recorded as the retention time, t_R. For injections of sample on the order of micro-liters (µLs), retention times for a given

constituent are constant regardless of sample concentration, given all other parameters are identical.[28] The volume of a given constituent in the sample is referred to as a band. When a band leaves the column, it is analyzed by the detector, and is represented as a peak in the chromatogram. The length of time the band exists is the peak width. The design parameters effecting the efficiency and fidelity of the chromatogram are shown in Table 1 adapted from Snyder *et al.*[28] Three major indicators of performance include the retention factor, selectivity, and plate number. The retention factor, k, is the ratio of the amounts of solute in the mobile phase and stationary phase; retention factors greater than 1 indicate the sample is engaged in strong physiochemical interactions with the stationary phase.[30] Additionally, the retention factor differs for each constituent within the sample, however when retention factors between varying sample constituents are similar, individual peaks become indiscernible, resulting in poor separation. The ratio of retention factor between two constituents refers to the selectivity, α. A measure of column efficiency or how well the HPLC is able to separate sample constituents is known as the plate number, NP. The plate number is proportional to the square of retention time over peak width, and generally should be greater than 2000.[31] Essentially, narrower peaks with selectivities far larger than 1 and retention factors between 2 and 10, indicate efficient and precise separation.[30] The instrument method summarizes the experimental conditions under which each sample and control blank samples (deionized water) were analyzed by HPLC.

Table 1: Impact of method design parameters on HPLC separation (adapted from Snyder *et. al.)*[28]

Parameter	Retention Factor, k	Selectivity, α	Plate Number, N
% of organic solvent	Major	Minor	Slight
Polarity of solvent	Minor	Major	Slight
Temperature	Minor	Minor	Minor
Column length	No effect	No effect	Major
Flow rate	No effect	No effect	Minor
Pressure	Slight	Slight	Minor

The instrument method for analysis was as follows: first, an injection purge for 6.5 minutes was done to reduce the risk of cross-contamination between earlier HPLC analyses. The column was then equilibrated for 35 minutes at a flow rate of 1 mL/min with a 50%-A mobile phase. Each sample is measured for 55

minutes, with an injection volume of 8.0 µL, at an operating temperature of 21.7 °C, a flow rate varied between 0.5 mL/min and 1.0 mL/min. After sample injection, the equilibration parameters are held for 20 minutes after which within 5 minutes, the flow rate was decreased from 1.0 mL/min to 0.5 mL/min while the mobile phase composition was decreased from 90%-A to 45%-A. In the next 20 minutes, the mobile phase composition was further decreased from 45% A to 5% A. Over the next 4 minutes, the flow rate was increased from 0.5 mL/min to 1.0 mL/min and held for 3 minutes. Over the final 2 minutes of the method, the mobile phase composition was increased from 5% A to 90% A. Before and after each sample injections, blank injections are done using the same instrument method as the samples to generate a measurement baseline. For the measurement of cRGDY on the surface of the cRGDY C' dots, absorbance at 275 nm was used (data not shown) and for measuring the cRGDY C' dot particles, absorbance at 647 nm was used as done in previous studies of C' dot characterization.[1,16] The PDA detector for each run is set to measure two distinct channels, absorbance at 275 nm and 647 nm with a resolution of 1.2 nm. The chromatograms were then normalized from 0 to 1; peak analysis was performed with an exponentially Modified Gaussian fit (Equation 14).[32] The exponential modification compensates for flow rate variations within the column, known as extra-column effects.[32] Here, A is the amplitude of a peak, τ is the exponential modifier (adjusting for extra-column effects) time constant, σ^2 is the Gaussian variance, t_R is the Gaussian center of gravity, and t′ is a dummy variable of integration.

Equation 14

$$f(t) = \frac{A(2\pi)^{-\frac{1}{2}}}{\tau\sigma}\int_0^{\infty} e^{\left[-\frac{(t-t_R-t')^2}{2\sigma^2}\right]} e^{\left[\frac{-t'}{\tau}\right]} dt'$$

Identified peaks were selected to represent early, middle, and late particle elution times, and integrated over an absorbance spectrum of 210-720 nm. The normalized absorbance spectra were plotted against peaks identified from un-fractionated HPLC chromatograms of C' dots not functionalized with cRGDY and containing only PEG on the surface (PEG C' dots). To identify trends in the peak height at 275 nm under the assumption that increases in absorbance at 275 nm was only due to cRGDY on the particle surface. Un-fractionated HPLC chromatograms were compared qualitatively for similarities in peak shape and elution time between each sample and to PEG C' dots.

RESULTS AND DISCUSSION

C' DOT SYNTHESIS

Having control over surface ligand density of C' Dot particles within a single batch may significantly enhance sample performance, and help with reproducibility issues from batch to batch reactions. Further, regulation of these characteristics may only be achieved by advanced characterization techniques. Synthesis and surface functionalization of C' dots in a batch reaction with control over surface ligands per particle distribution is difficult and with current techniques unlikely to be consistent or reproducible.[5] Due to the unknown number of binding sites per particle and the high binding affinity of the silica surface to cRGDY peptide, a large fraction of the total cRGDY may bind to very few particles before cRGDY can diffuse throughout the entire reaction volume to reach particles further from the entry point of cRGDY. The resulting distribution would differ substantially from a Gaussian distribution expected for a stochastic process.[33] Incomplete conjugation of Maleimide-PEG-Silane to cRGDY or free PEG-Silane in the reaction volume may also interfere with the reaction kinetics of cRGDY binding, which could further contribute to a divergence from ideal Gaussian distributions of cRGDY per particle. As shown by Ma *et. al.*, variances in PEG concentration impact PEG density on the C' dot surface, thereby affecting the binding of other surface ligands, the hydrodynamic radius, the particle surface charge, and the particle stability in solution (susceptibility to aggregation).[1] Apart from reaction conditions, variations in GPC elution times and peak symmetries are related to manual loading of the sample onto the GPC column. Injection of a sample assumed to have heterogeneous surface functionalization, onto the GPC column, which is packed with gel with a non-uniform top surface, may result in disturbed peak curves, and skewed particle distributions, and over-loading of the column with large particle volumes increases the skewness even further. Characterization measurements may also be affected by what fractions are collected from the chromatograms. As shown in Figure 2 depending on which elusion time window is collected, the sample could contain more or less dyed or undyed aggregates, which in effect may alter hydrodynamic radius measurements, number of dyes per particle, distribution, and average number of cRGDY per particle.

GPC RESULTS

Based on the SEC properties of GPC, aggregates and free dyes are observable in the first chromatogram as each impurity elutes before and after the main cRGDY C' dot peak, respectively. Shown in Figure 4 and Figure 5 are stacked chromatograms of the 120 μL cRGDY and 60 μL cRGDY C' dot samples, respectively. Each sample differed only in the total volume of cRGDY (~21 μM) added to the sub-10 nm silica nanoparticle synthesis reaction volume, while all other experimental parameters were assumed constant across the two samples. Thus 120 μL of cRGDY (2.5 nM final) was used for the 120 μL cRGDY C' dot sample; for the 60-μL cRGDY C' dot sample, 60-μL of cRGDY (1.3 nM final) were applied. Observations from the post synthesis purified samples show a significant peak between 9 and 10 minutes for both the 120 μL and 60 μL cRGDY C' dot samples, which is indicative of silica aggregates of significantly larger molecular masses compared to the cRGDY C' dot particles. Based on observation of both aggregate peaks, silica aggregates appear to be relatively monodisperse, and exhibit a Gaussian distribution at resolutions attainable by GPC. Additionally, skewness in the silica aggregate peaks are observable in both samples, which may provide some evidence that the population of aggregate particles could include other species (possibly large aggregates of un-conjugated PEG) or sub-populations of aggregate sizes; however, these claims cannot be substantiated solely from GPC. The second, and main peak to elute around 15 minutes is associated with the cRGDY C' dot particles for both 120 μL and 60 μL cRGDY C' dot samples. From the post-synthesis chromatograms, an elution window was taken to separate the cRGDY C' dot particle from aggregates and free dyes, thereby purifying the samples. Eluates were collected between 13 and 17.5 minutes (Figure 4, top). The fractions were up-concentrated with a spin filter at 4270 RPM for 45 minutes, and loaded onto the GPC column to generate the purified chromatogram (Figure 4, bottom). From the purified chromatogram, an elution window between 13 and 16 minutes was collected to further ensure the best possible homogenous sample of cRGDY C' dots with respect to size and surface ligand density per particle. Similarly, with the 60 μL cRGDY C' dot sample, an elution window between 12 and 18 minutes was collected from the post-synthesis chromatogram (Figure 5, top). From the purified sample (Figure 5, bottom) an elution window between 13 and 19 minutes was taken. Table 2 shows the elution windows for three fractions (shown as shaded regions in Figure 4, bottom and Figure 5, bottom) taken from each sample at early, middle and late times of the GPC elugrams. Un-fractionated samples of the 120 μL and 60 μL

cRGDY C’ dots were taken for HPLC analysis from a previous GPC purification, which yielded a similar GPC chromatogram (not shown here).

Table 2: Elution windows from GPC chromatograms of sample fractions

Sample	Fraction	Elution Window (minutes)
120 µL cRGDY C’ dots	1	13.9-14.2
	2	15.1-15.4
	3	16.6-16.9
60 µL cRGDY C’ dots	1	13.7-14.0
	2	15.2-15.5
	3	16.4-16.7

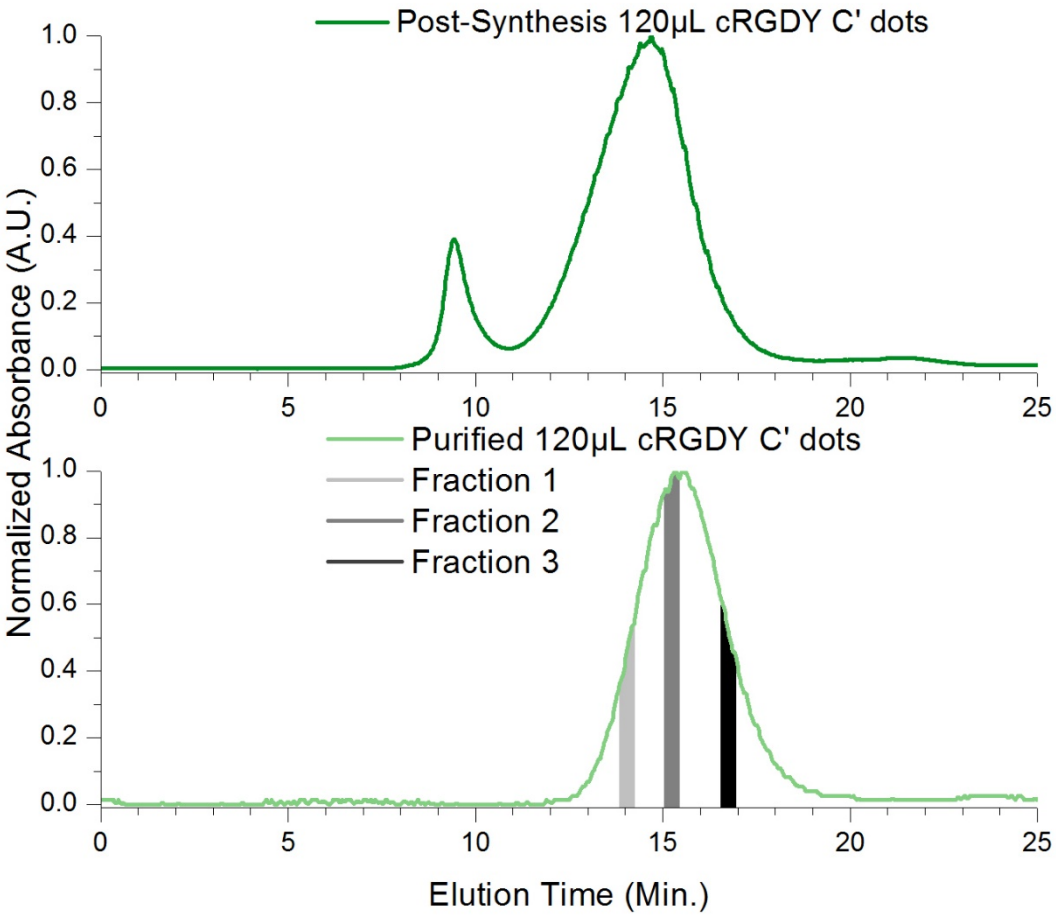

Figure 4: GPC Chromatograms of post-synthesis (top) and purified (bottom) 120 µL cRGDY C' dots

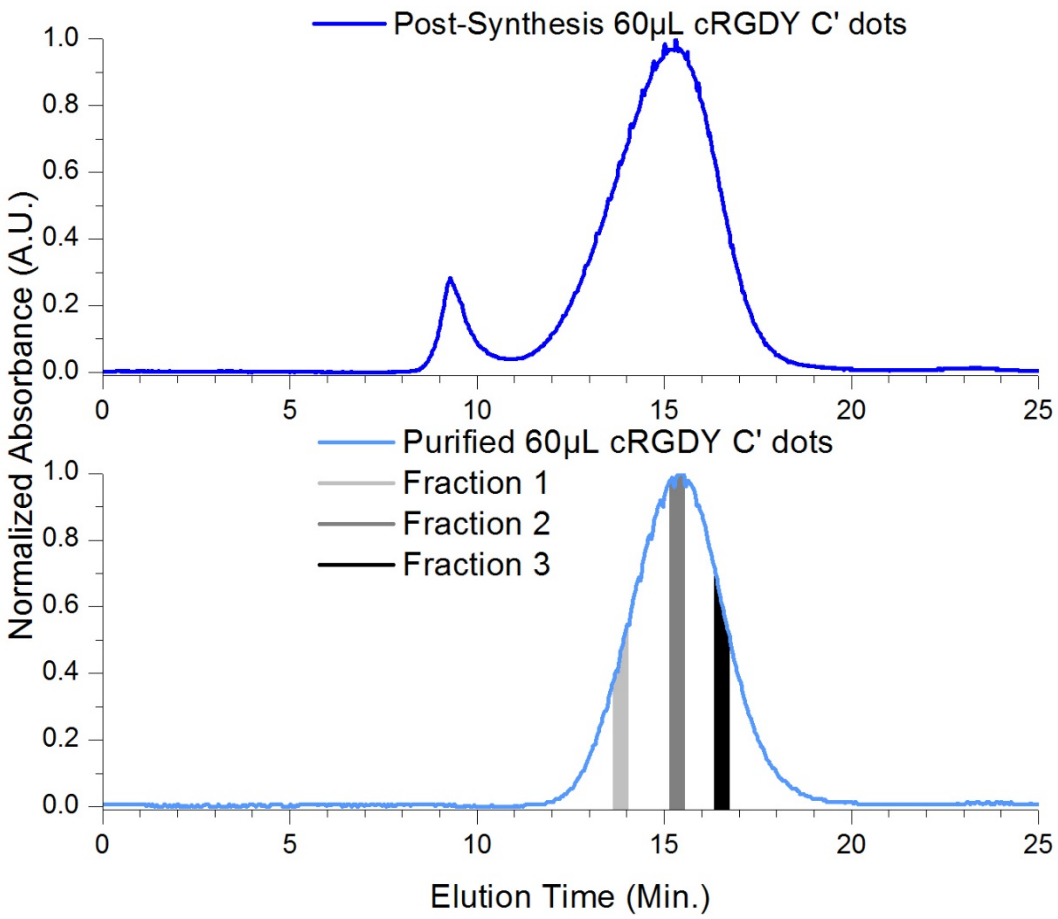

Figure 5: GPC Chromatograms of post-synthesis (top) and purified (bottom) 60 µL cRGDY C' dots

Observation of elugrams of both samples shows peak roughness and skewness. The roughness is most likely due to variations in manually loading the samples onto the column (discussed in the C' dot Synthesis Results section). Observation of a slight skewness to the left in the elugrams for both purified samples suggests the presence of sub-populations. The sub-populations could result from varying surface ligand per particle distributions and surface ligand densities, which were further investigated with HPLC.

FCS RESULTS

The normalized autocorrelations with triplet state corrections in the fits of each of the two samples are shown against Cy5 free dye and the respective fit functions in Figure 6 and Figure 7. Equation 15 was used to normalize the autocorrelation fit and data.

Equation 15

$$G(\tau)_{Normalized} = (G(\tau) - 1) * N$$

Here $G(\tau)$ represents averaged autocorrelation data from three FCS runs and N is the average number of C' dots or Cy5 dye molecules within the focal volume.

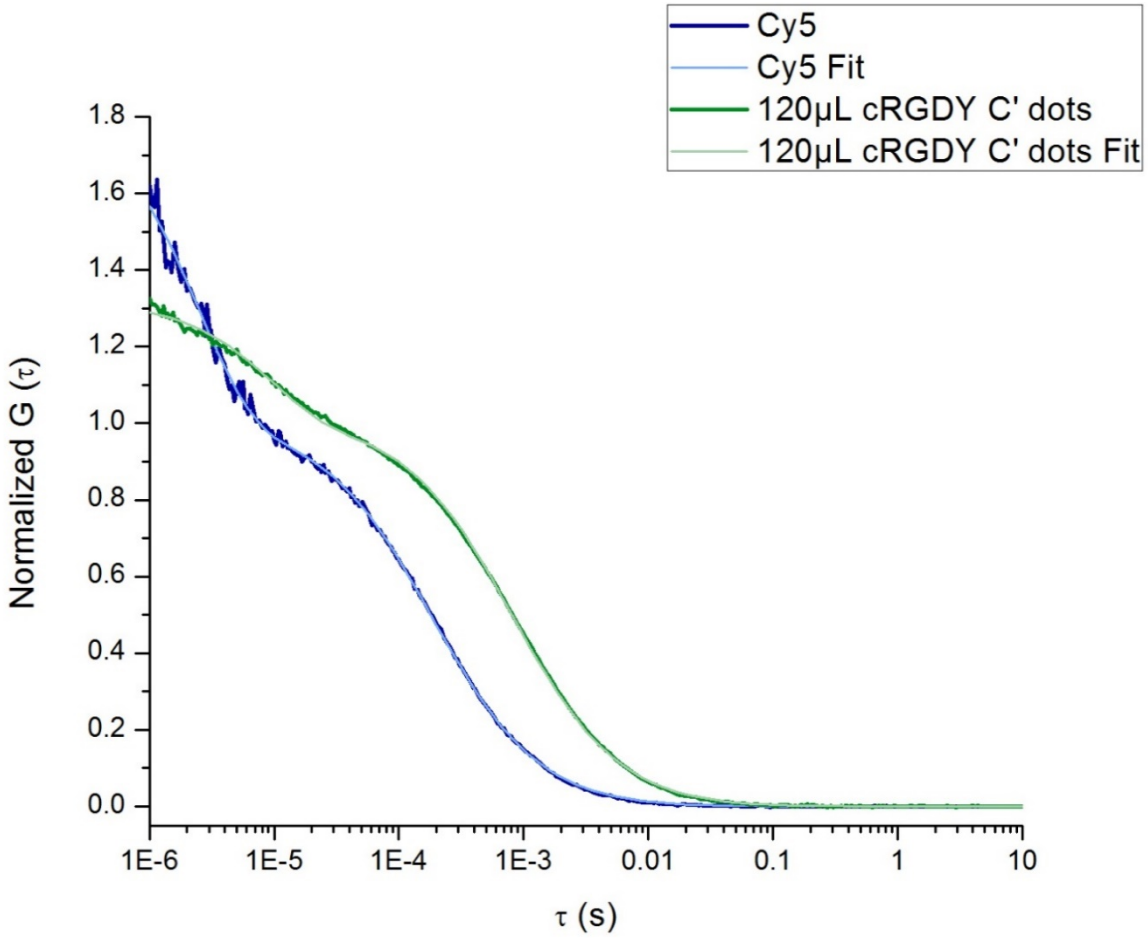

Figure 6: Normalized FCS autocorrelation data and fit of the 120 µL cRGDY C' dot sample and free Cy5

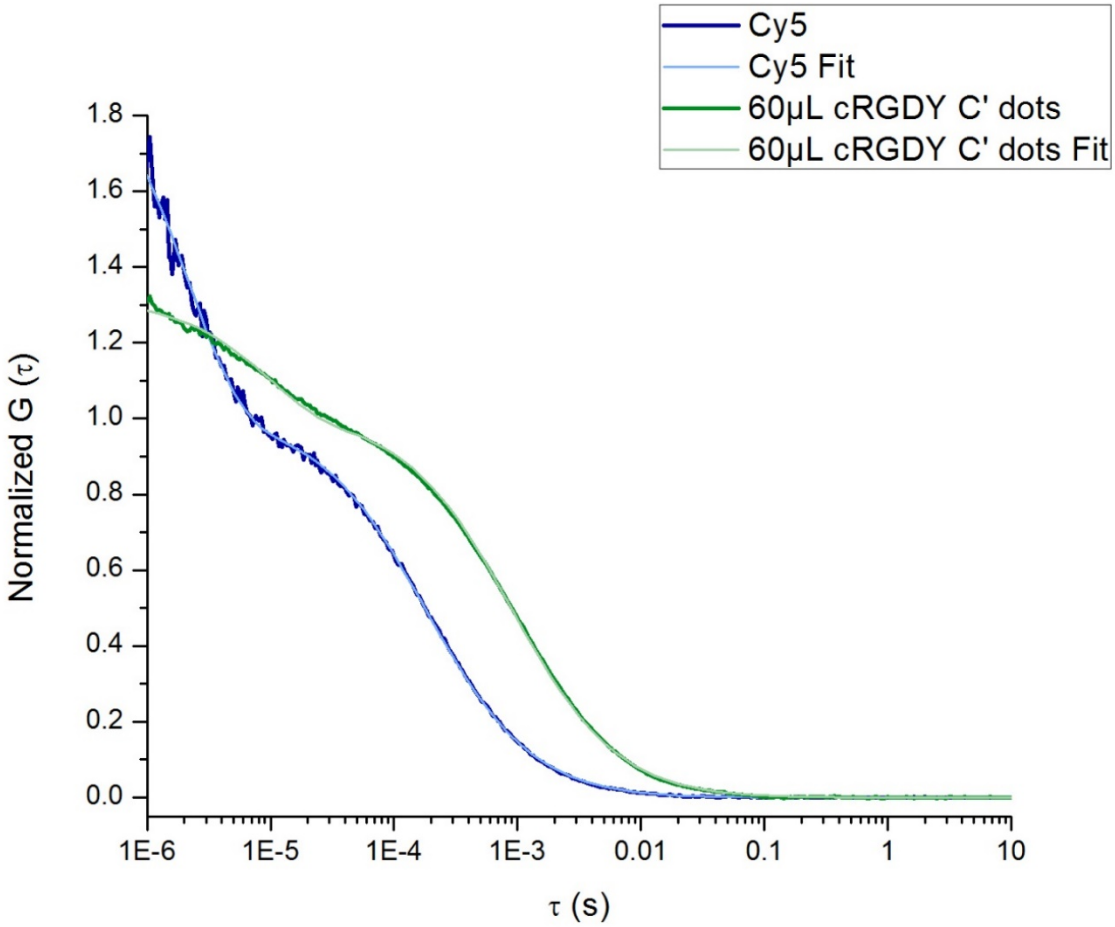

Figure 7: Normalized FCS autocorrelation data and fit of the 60 µL cRGDY C' dot sample and free Cy5

Several features of the curves indicate various phenomena based on time scale. At short time scales (10^{-7}-10^{-5}), rotational diffusion and triplet state phenomena dominate while at longer time scales (10^{-5}-10^{1}) translational diffusion phenomena are observable.[34] For the purpose of this study, only triplet state and translational diffusion phenomena are measured and accounted for in the autocorrelation fit function. In Figure 6 and Figure 7, both samples exhibit a reduction in triplet state phenomena at short time scales, and transition to longer translational diffusion time, which is expected considering that the cRGDY C' dots are considerably larger than free dye molecules and the encapsulation of dye by the silica core reduces the population of dyes in the triplet state. Both 120 µL and 60 µL cRGDY C' dot samples exhibit similar autocorrelation curves, with a slight difference in the translational diffusion time scale as shown by the inlay of Figure 8.

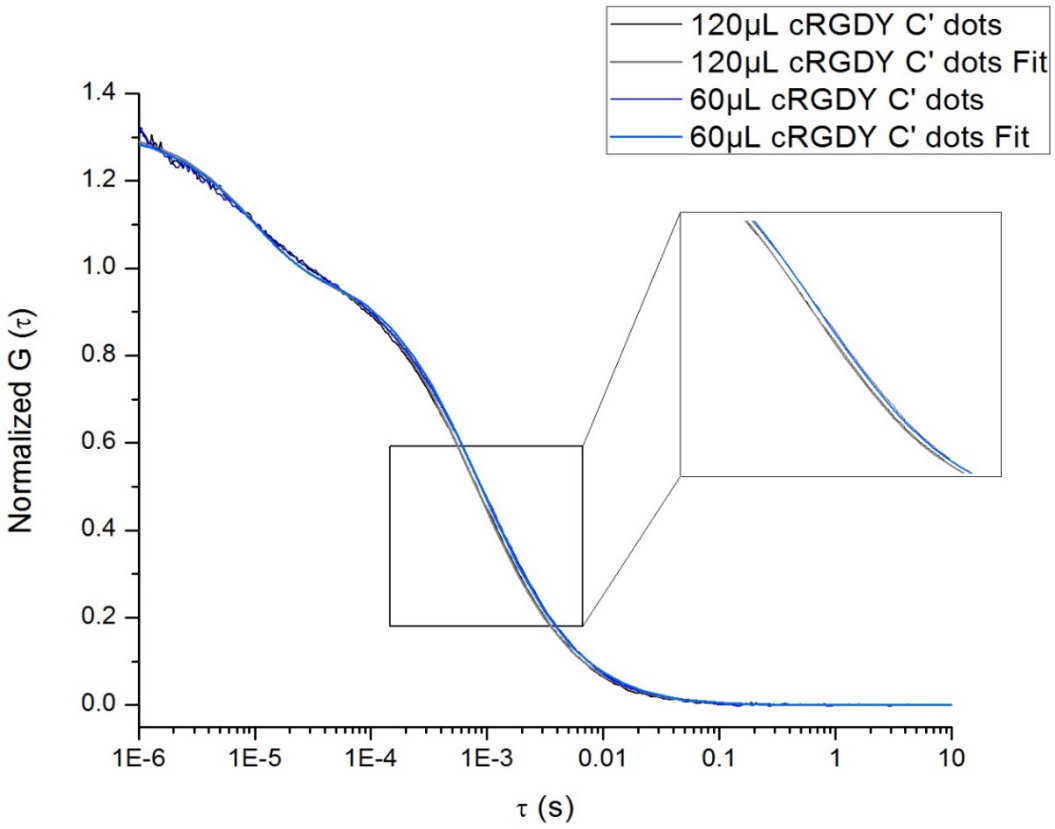

Figure 8: Normalized FCS autocorrelation data and fit functions of the 120 µL cRGDY and 60 µL cRGDY C' dot samples

From the FCS autocorrelation fits as well as independent absorbance data, several characteristics of cRGDY C' dot particles are obtained, which include hydrodynamic diameter and sample concentration from FCS, and average dyes per particle and average cRGDY per particle from the combination of FCS and absorbance measurements. Results are summarized in Table 3, and describe average dyes per particle and cRGDY ligands per particle numbers. For the purpose of improved particle characterization, information regarding cRGDY per particle distributions would be highly desirable, but is not accessible from these analyses.

Table 3: 120-µL cRGDY and 60-µL cRGDY C' dot sample characteristics

Sample Name	Concentration of Sample (µM)	Average Hydrodynamic Diameter per Particle (nm)	Average Cy5 per Particle	Average cRGDY per Particle
120-µL cRGDY C' dots	27	6.2	1.8	17
60-µL cRGDY C' dots	110	6.7	1.8	15

UV/VIS RESULTS

Absorbance spectra of free Cy5 dye, PEG C' dots and cRGDY C' dots for each sample (120 µL and 60 µL cRGDY C' dots) absorbance matched to Cy5 dye are shown in Figure 9 and Figure 10, respectively.

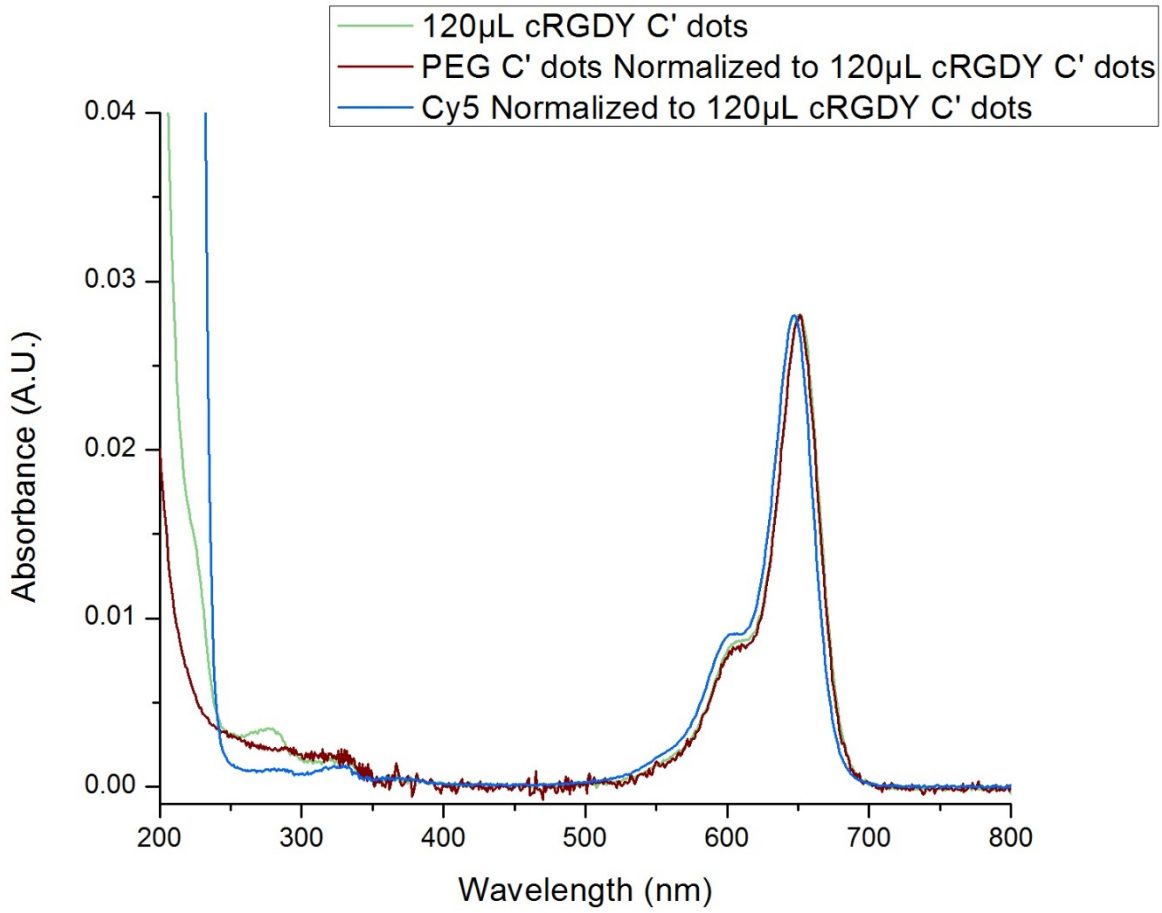

Figure 9: Absorbance spectra of 120 µL cRGDY C' dots, PEG C' dots and free Cy5 dye normalized to Cy5 dye absorption.

The absorbance peak of free Cy5 dye appears at around 647 nm, C' dots with Cy5 dye and/or cRGDY shows this absorption peak around 650 nm, which is characteristic of two or more dye molecules oriented closely to one another and parallel (red shift). This orientation enables strong coupling interaction conditions that result in the shouldering seen from Cy5 at 600 nm known as the hypsochromic band (H-band).[35] The absorbance peak for free cRGDY and cRGDY on the surface of C' dots appears around 275 nm.[16]

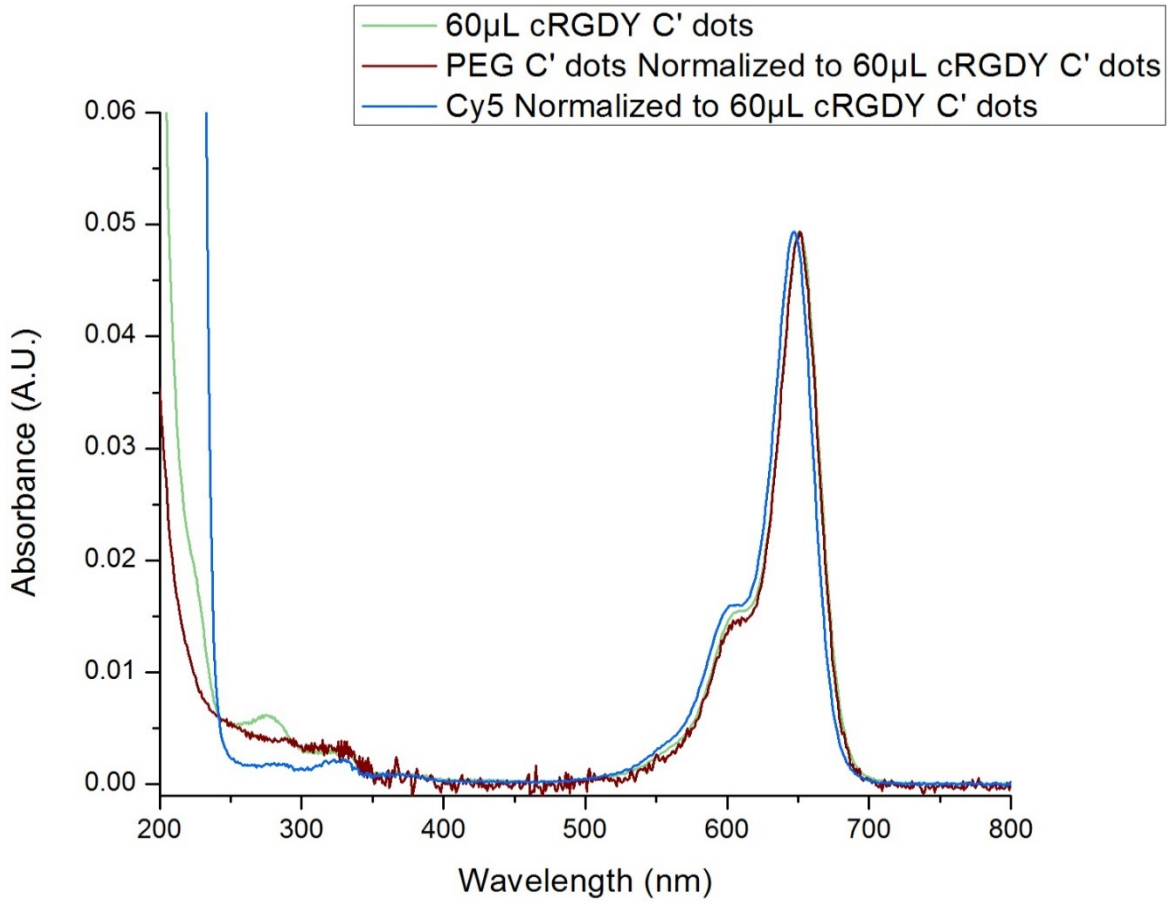

Figure 10: Absorbance spectra of 60 µL cRGDY C' dots, PEG C' dots and free Cy5 dye normalized to Cy5 dye absorbance.

For both samples, the cRGDY peak at 275 nm is larger compared to PEG C’ dots, indicating the presence of cRGDY on the surface of each particle (see also Table 3 of the previous section). In order to obtain the average number of cRGDY per particle, the dye absorbance spectra of C’ dots and cRGDY C’ dots are normalized and then the absorbance of C’ dots at 275 nm is subtracted from the absorbance of the cRGDY C’ dots at 275 nm. This difference is used to calculate the average number of cRGDY per particle from a calibration with free cRGDY and from the particle concentration information generated from FCS measurements. A comparison between the normalized absorbance spectra of 120 µL, and 60 µL cRGDY C’ dots, is shown in Figure 11 to qualitatively observe the height difference of the cRGDY peak at 275 nm.

In Figure 11, there is an increased absorption at 275 nm for the 120 µL cRGDY C’ dot sample indicating more cRGDY present, on average, than in the 60 µL cRGDY C’ dot sample; Indeed, using FCS concentration information corroborated the 120 µL cRGDY C’ dot sample to have 2 more cRGDY per particle on average.

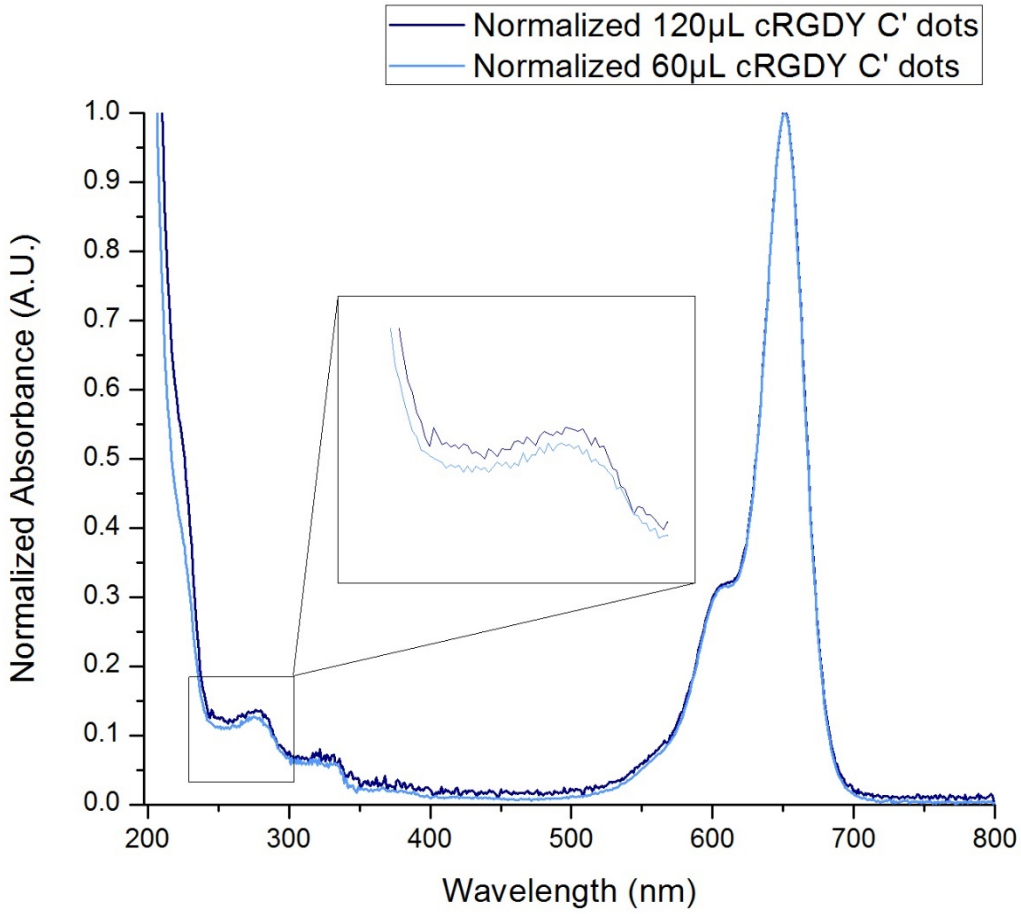

Figure 11: Absorbance spectra comparison of normalized 120 µL and 60 µL cRGDY C' dots

C’ DOT HPLC CHARACTERIZATION

HPLC runs were performed on GPC fractions of each of the 120-μL and 60-μL cRGDY C’ dot samples, shown as shaded regions under the GPC chromatograms in Figure 4 (bottom) and Figure 5 (bottom), respectively. The HPLC chromatograms presented in this section were obtained using the 647 nm wavelength channel, where Cy5 dye encapsulated within the particles absorb. Therefore, observed peaks are assumed to contain C’ dots as it is presumed that no other chemical in the sample absorbs significantly at this wavelength. In Figure 12, HPLC chromatograms for the two un-fractionated 120 μL and 60 μL cRGDY C’ dot synthesis batches are compared to each respective sample fractions.

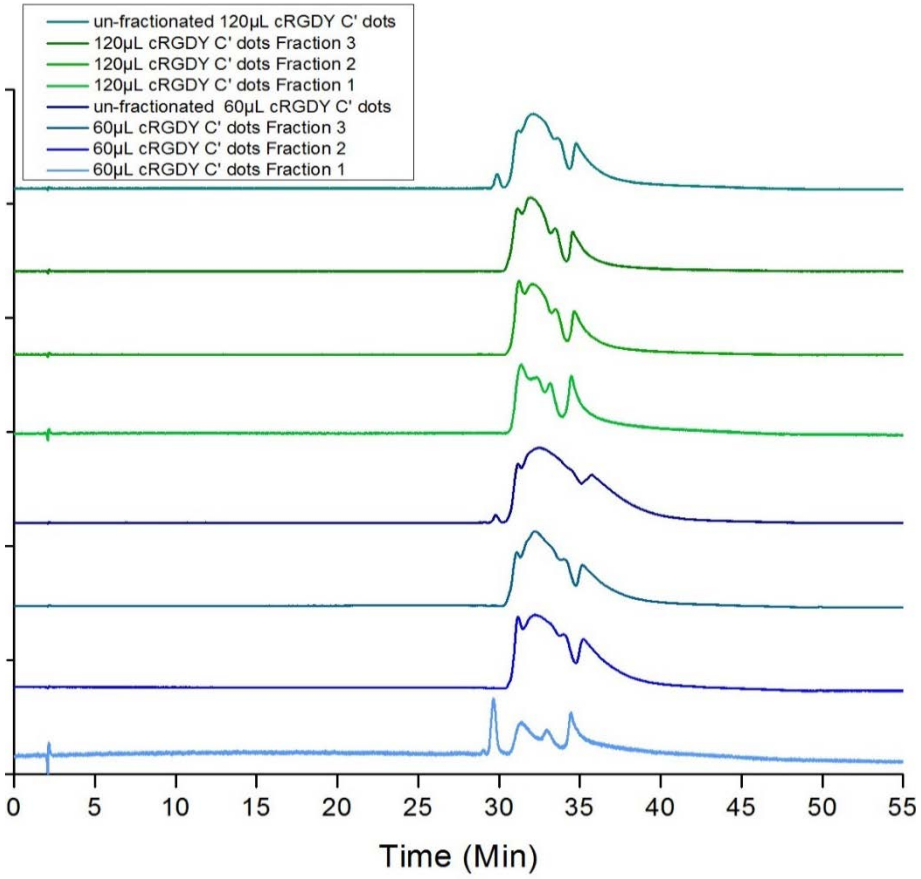

Figure 12: Stacked chromatograms of un-fractionated and fractionated 120 μL and 60 μL cRGDY C' dot samples. Shown in shades of blue are the 60 μL cRGDY C’ dot sample (darkest blue) and fractions. Similarly, depicted in shades of green are the 120 μL cRGDY C’ dot samples

From Figure 12 many of the main features as a function of elution time of the HPLC peaks are conserved across samples and fractions, indicating that the particles of all fractions engaged in similar interactions with the column. An interesting feature comparing un-fractionated and fractionated samples is the peak

broadening that is apparent in the un-fractionated samples. Broader peaks signify an increased heterogeneity of particle populations under the peak; most likely, a result of surface ligands per particle variances, due to both particle size dependent distributions (larger particles could have higher surface ligand numbers simply because of increased surface area). Sample fractioning was implemented to minimize size dependent contributions to surface ligand number variations per particle in consideration of the complexity of elucidating both size dependent and size-independent contributions to ligand distributions.

For clarity, elugrams of the un-fractionated 120 µL and 60 µL cRGDY C' dot samples and their respective fractions are plotted separately between 25 and 45 minutes elution time, in Figure 13 and Figure 14, respectively. In Figure 13 for the 120 µL cRGDY C’ dot sample and its fractions; note the shoulders on either side of the main peak at 32 minutes of the un-fractionated sample. While in fraction 1 these shoulders are more differentiated from the peak at 32 minutes compared to the un-fractionated sample, this difference decreases with increasing fraction.

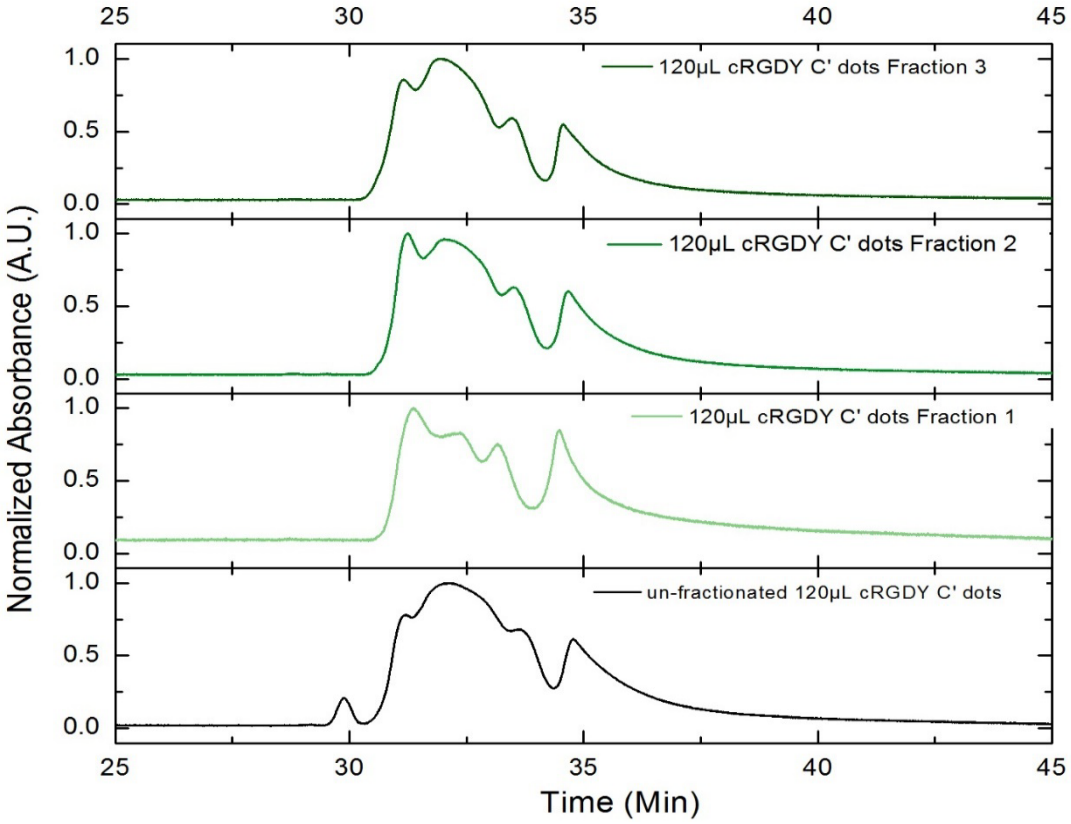

Figure 13: Stacked normalized HPLC chromatograms of fractionated and un-fractionated 120 µL cRGDY C' dots

Another feature observed in the un-fractionated sample is the small peak at 30 minutes, which is not present in any of the fractions. This peak is most likely due to an impurity that was separated from the fractions during the GPC fractionation. Similarly, the stacked plots of the 60 µL cRGDY C' dot HPLC chromatograms show a comparable trend to the 120 µL cRGDY C' dot fractions, with the exception of the 60 µL cRGDY C' dot/fraction 1 showing a significant peak at 29.7 minutes.

120 µL and 60 µL cRGDY C' dot fractions 1

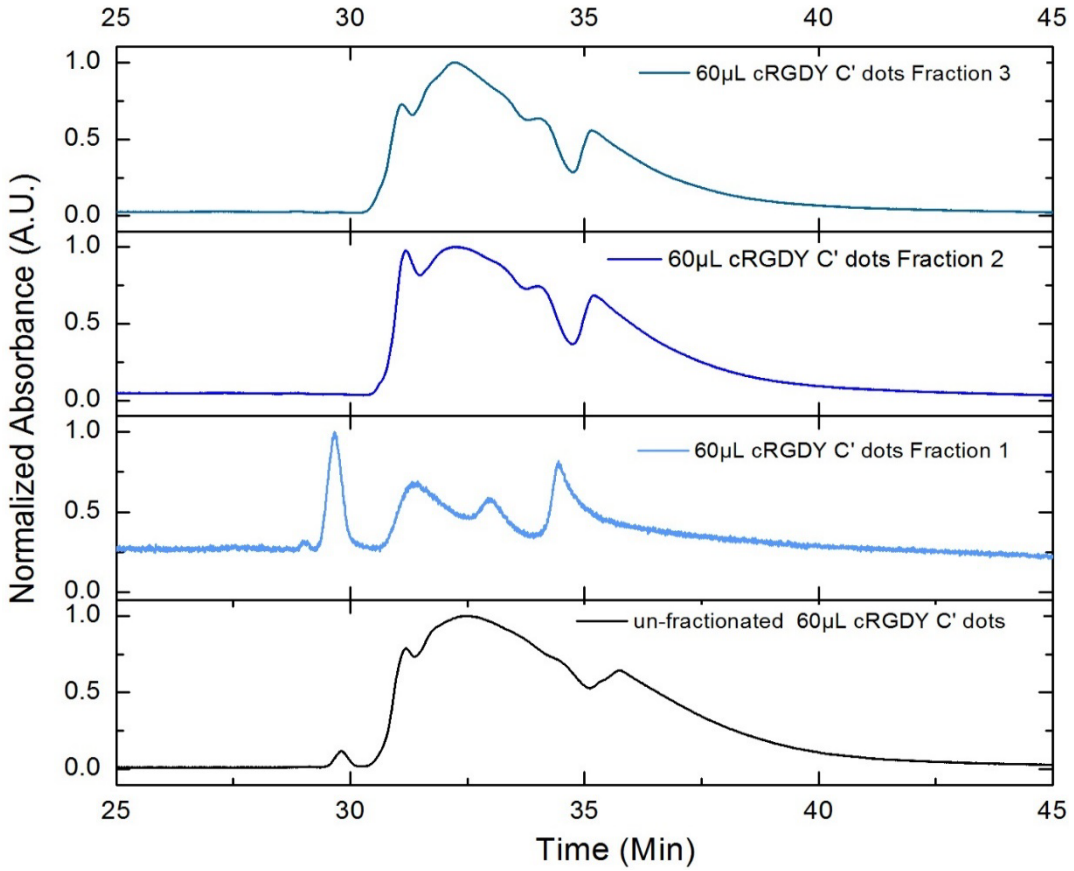

Figure 14: Stacked normalized HPLC chromatograms of fractionated and un-fractionated 60 µL cRGDY C' dots

Each HPLC elugram was quantitatively analyzed by fitting with Modified Gaussian functions in order to discern discrete contributions to the overall particle population of cRGDY surface modified particles (Figure 15). The area under each peak was then integrated for comparison. Furthermore, rather than only using the 647 nm channel, the entire absorbance spectra from the photodiode array detector (PDA) were qualitatively analyzed at different peak positions of the elugrams. Figure 15 shows the Modified Gaussian

fits for fractions 1 of the 120 µL and 60 µL cRGDY C' dot samples, respectively, and Table 4 contains elution times for each of the four peaks observed. Across both samples, peaks at about 31, 33 and 35 minutes are conserved, while fraction 1 of the 60 µL cRGDY C' dot sample contains a unique peak around 30 minutes. This peak also appears in the un-fractionated sample but does not appear in any other fraction. Additionally, fraction 1 the 120 µL cRGDY C' dot sample shows a peak around 32 minutes, not present in the 60 µL cRGDY C' dot sample. This could indicate an additional population of particles with unique surface chemistry due the increased concentration of cRGDY. Overall, fits appear to appropriately model each peak despite the height differences in the baseline due to the tailing effects.

The full PDA absorbance spectra for each peak position of the two samples are shown in Figure 16. They reveal that peak 1 of fraction 1 of the 60 µL cRGDY C' dot sample does not contain an ensuing peak at 275 nm that would be indicative of the presence of cRGDY, nor significant scattering at wavelengths below 275 nm expected for a (PEGylated) particle. The sample nonetheless contains an absorption peak, and H-band shoulder, consistent with Cy5 dye. Due to missing feature signals from both cRGDY and PEGylated particles, this peak most likely represents free Cy5 dye and not C' dots. The remaining absorbance spectra across both samples, with the exception of 120 µL cRGDY C' dot peak 2/fraction 1 and cRGDY C' dot peak 3/fraction 1, share similar absorbance spectra, suggesting that similar material was eluted. The inconsistencies between the two samples for the two aforementioned peaks perhaps highlight a differentiation in the distribution of surface ligands across the two samples. Alternatively, these differences are not present in the other fractions and may be a result from the atypical low signal to noise ratio present only in the 60 µL cRGDY fraction 1 sample. For both samples an additional feature appears, a shoulder at 225 nm, which was not apparent in the un-fractionated sample absorbance spectra (Figure 9 and Figure 10). This shoulder is indicative of tyrosine conjugated to peptides, such as cRGDY.[36] The peaks at 31 minutes appear to exhibit a stronger signal of the speculated cRGDY marker, which decreases at later elusion times presenting lower peaks with the exception of 60 µL cRGDY C' dot peak 3. In contrast, the un-fractionated sample absorbance spectra, the 60 µL cRGDY C' dot sample exhibits a higher signal at 275 nm than for the 120 µL cRGDY C' dot sample. The origin of this signal is unclear considering the 120 µL cRGDY C' dot sample was shown to contain more cRGDY per particle on average from absorbance and FCS measurements. This pattern is also observed for fractions 2 and 3, see Figure 18 and Figure 20.

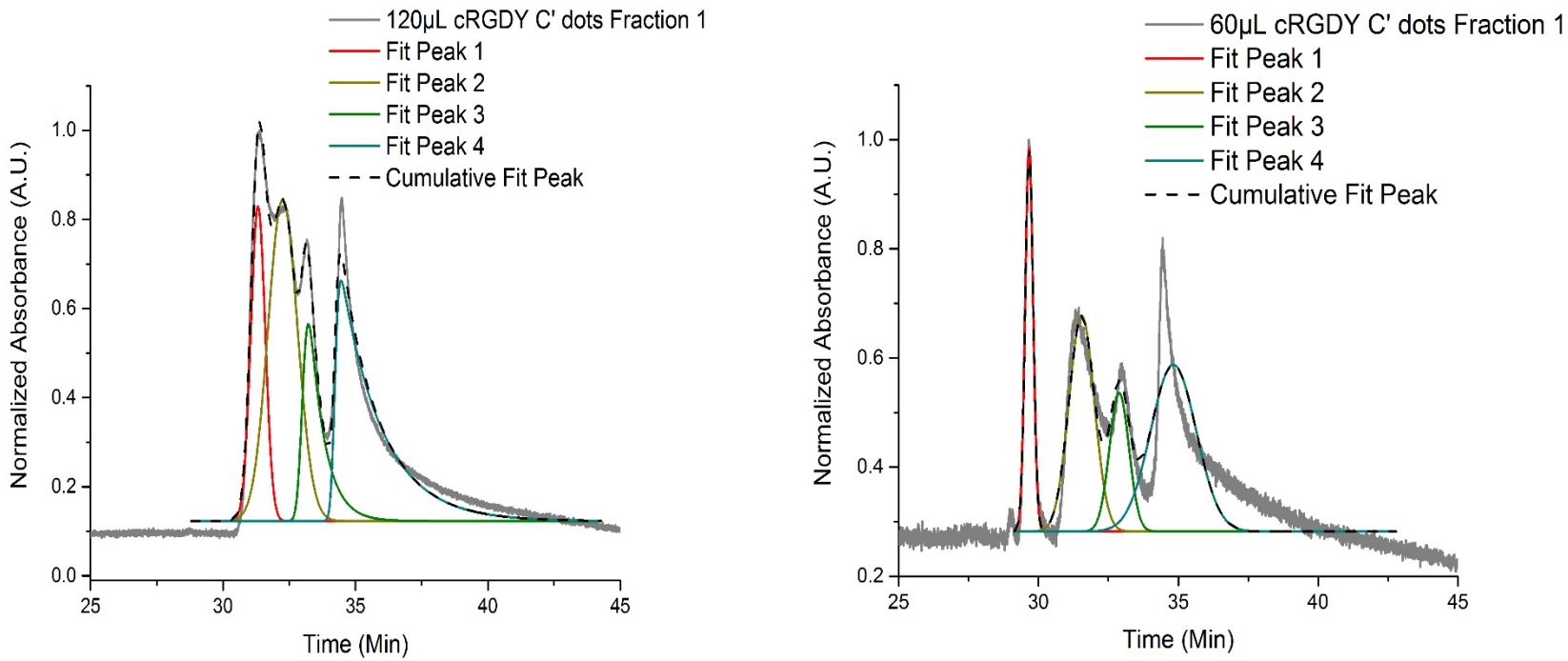

Figure 15: Modified Gaussian fit of normalized HPLC chromatogram for 120 μL (left) and 60 μL (right) cRGDY C' dot samples from GPC fractions 1 (see Figures 4 and 5 for comparison)

Table 4: 120 μL and 60 μL cRGDY C’ dot GPC fractions 1 HPLC chromatogram peaks with corresponding peak elution times

Sample	Peak	Elution Time (minutes)
120 μL cRGDY C’ dots GPC Fraction 1	1	31.3
	2	32.4
	3	33.2
	4	34.5
60 μL cRGDY C’ dots GPC Fraction 1	1	29.7
	2	31.3
	3	33.0
	4	34.5

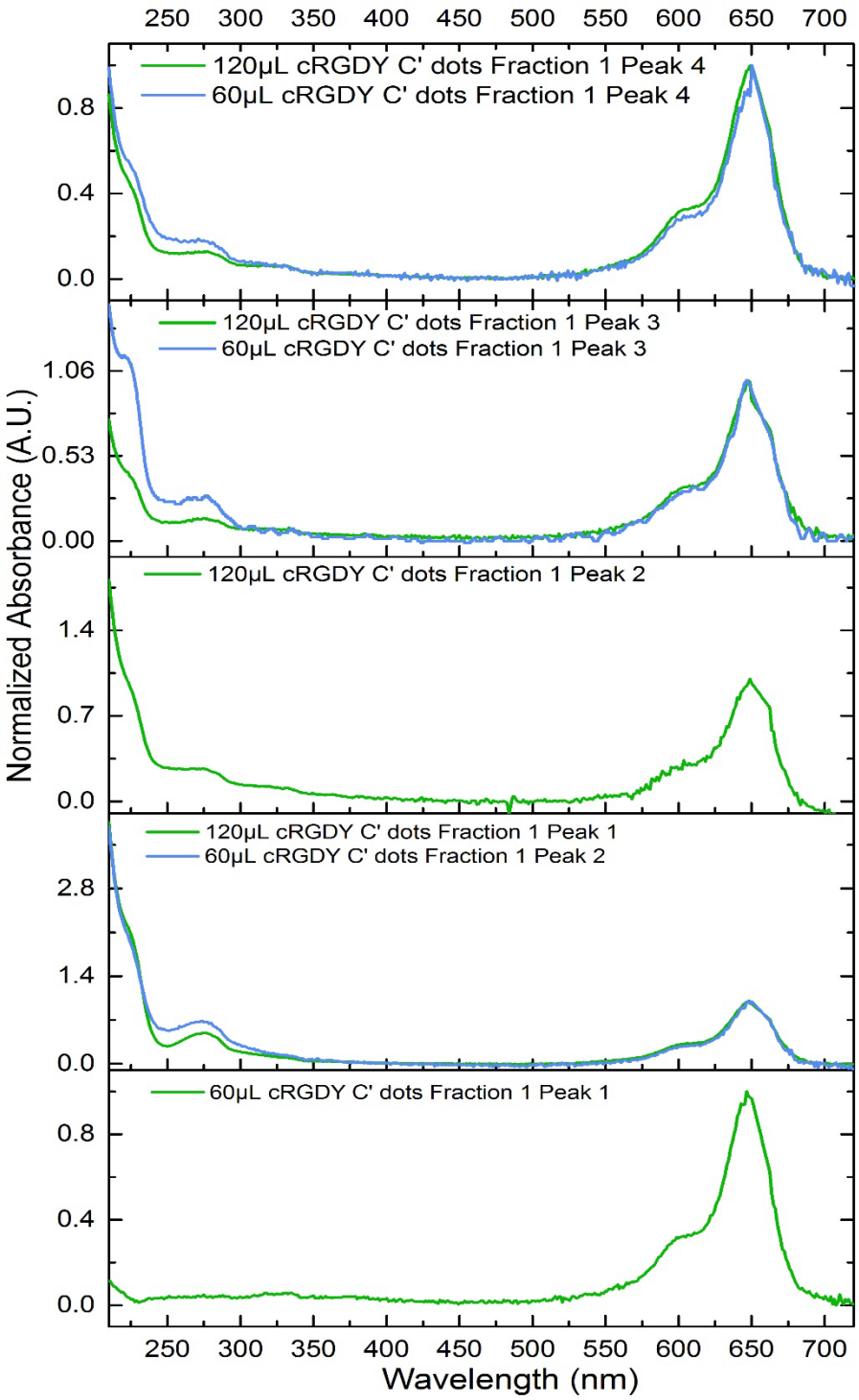

Figure 16: A stack plot of normalized absorbance spectra of HPLC chromatogram of fraction 1 peaks for 120 μL and 60 μL cRGDY C' dots GPC sorted by corresponding peak elution times for appropriate comparison.

120 µL and 60 µL cRGDY C' dot fractions 2

Figure 17 and Table 5 show the Modified Gaussian data fits and peak elution times, respectively, for fractions 2 of the 120 µL and 60 µL cRGDY C' dot samples. The fits for Figure 17 more closely match the baseline, and both samples share similar peak features and elution times.

The full PDA derived absorbance spectra associated with each peak of the fractions 2 are very similar for both C' dot samples. As was the case for fractions 1, the highest cRGDY signal appears for peak 1 at 31 minutes and decreases with increasing elution time for both samples, i.e. with increasing fraction number. This suggests that particles with higher cRGDY numbers on the surface move faster through the HPLC column. Interestingly, as elution times increase, the Cy5 signal increases. This observation may indicate an increase in particle numbers over elution time and supports the hypothesis that fewer particles may have a pointedly larger amount of cRGDY on the surface, while the majority of the population contains very little. Thereby, exhibiting a highly skewed distribution by deviating the distribution of cRGDY per particle away from an ideal Gaussian distribution. The shoulder at 225 nm increases for the 120 µL cRGDY C' dot sample as elution time increases. How changes in the signal at 225 nm reflect varying amounts of cRGDY is unclear, and nontrivial.

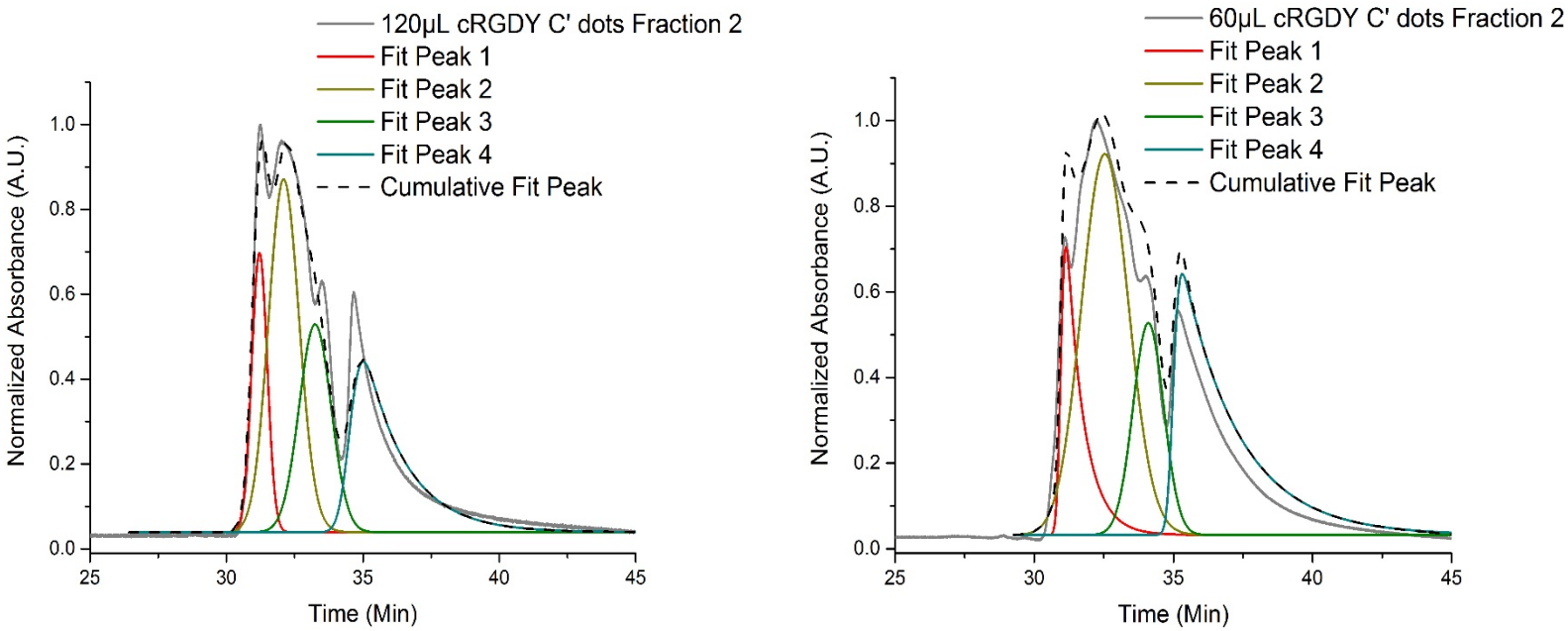

Figure 17: Modified Gaussian fit of normalized HPLC chromatogram for 120 µL (left) and 60 µL (right) cRGDY C' dot samples from GPC fractions 2 (see Figures 4 and 5 for comparison)

Table 5: 120 µL and 60 µL cRGDY C’ dot GPC fractions 2 HPLC chromatogram peaks with corresponding peak elution times

Sample	Peak	Elution Time (minutes)
120 µL cRGDY C’ dots GPC Fraction 2	1	31.3
	2	32.0
	3	33.5
	4	34.7
60 µL cRGDY C’ dots GPC Fraction 2	1	31.2
	2	32.4
	3	34.0
	4	35.2

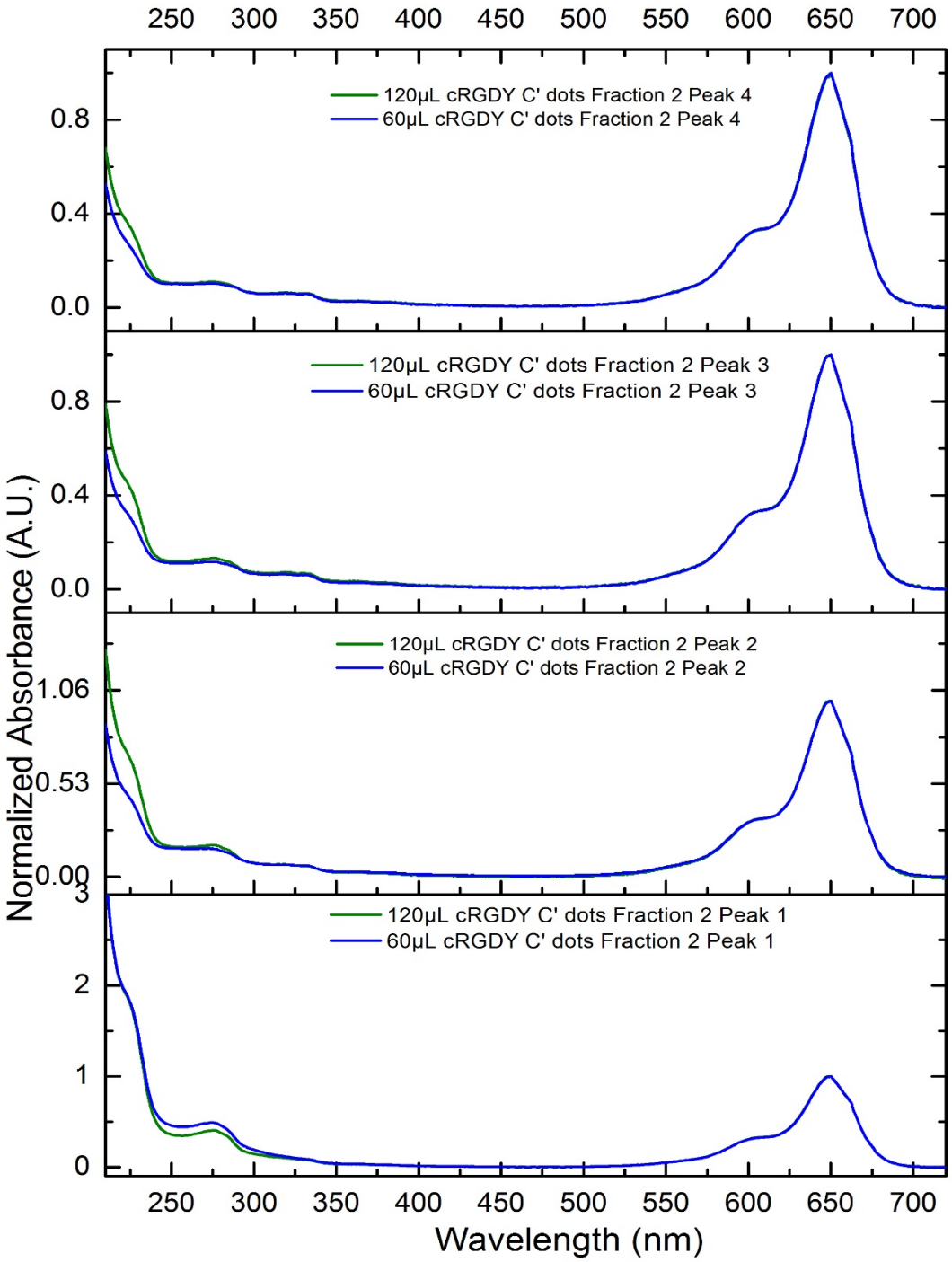

Figure 18: A stack plot of normalized absorbance spectra of HPLC chromatogram of fraction 2 peaks for 120 μL and 60 μL cRGDY C' dots GPC sorted by the matching peak elution times for appropriate comparison.

120 µL and 60 µL cRGDY C' dot fractions 3

For fraction 3 of the 120 µL and 60 µL cRGDY C' dots samples, Figure 19 and Table 6 show the Modified Gaussian fits and peak elution times, respectively. The Modified Gaussian fits appear to conform to the chromatogram appropriately; both samples share similar peak features and elution times (see Figure 19).

The full PDA derived absorbance spectra of fraction 3 samples exhibit similar patterns to the fraction 2 samples: the highest cRGDY signal appears at early elution times and decreases with increasing elution time, i.e. peak number. The similarity between fractions highlights a rather important observation, that the surface ligand particle populations appear not to be size dependent.

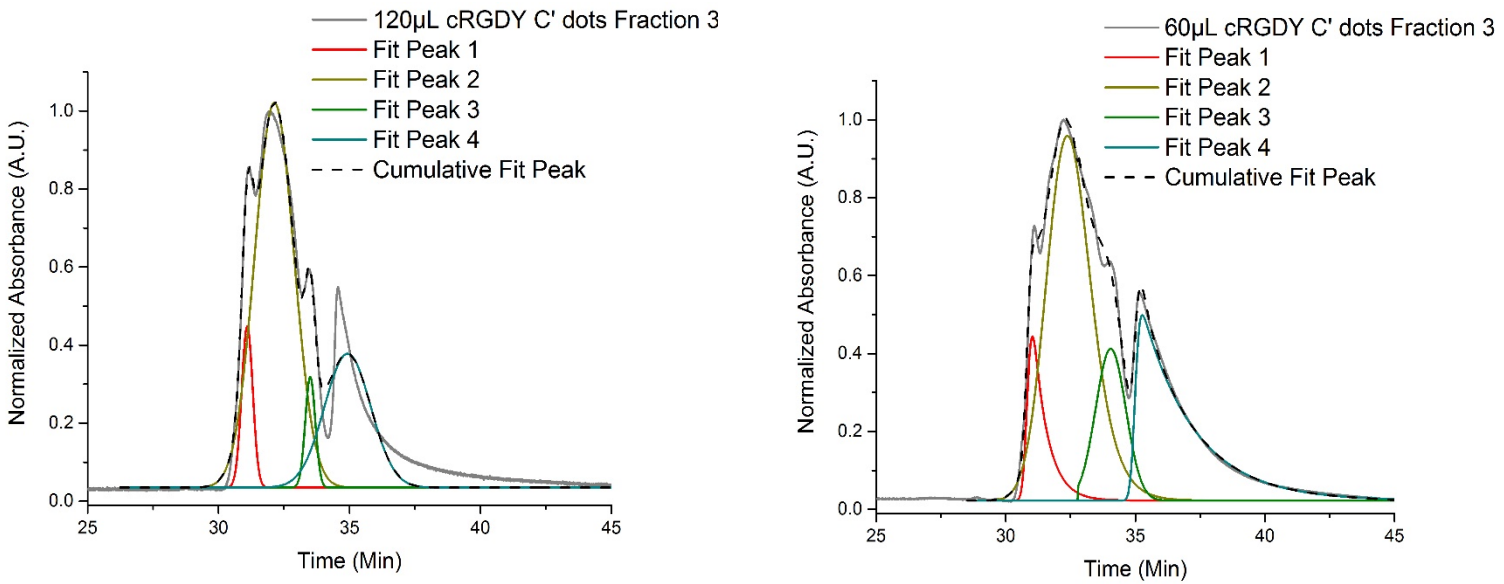

Figure 19: Modified Gaussian fit of normalized HPLC chromatogram for 120 µL (left) and 60 µL (right) cRGDY C' dot samples from GPC fractions 3 (see Figures 4 and 5 for comparison)

Table 6: 120 µL and 60 µL cRGDY C’ dot sample GPC fractions 3 HPLC chromatogram peaks with corresponding peak elution times

Sample	Peak	Elution Time (minutes)
120 µL cRGDY C’ dots GPC Fraction 3	1	31.2
	2	32.0
	3	33.5
	4	34.6
60 µL cRGDY C’ dots GPC Fraction 3	1	31.1
	2	32.2
	3	34.0
	4	35.2

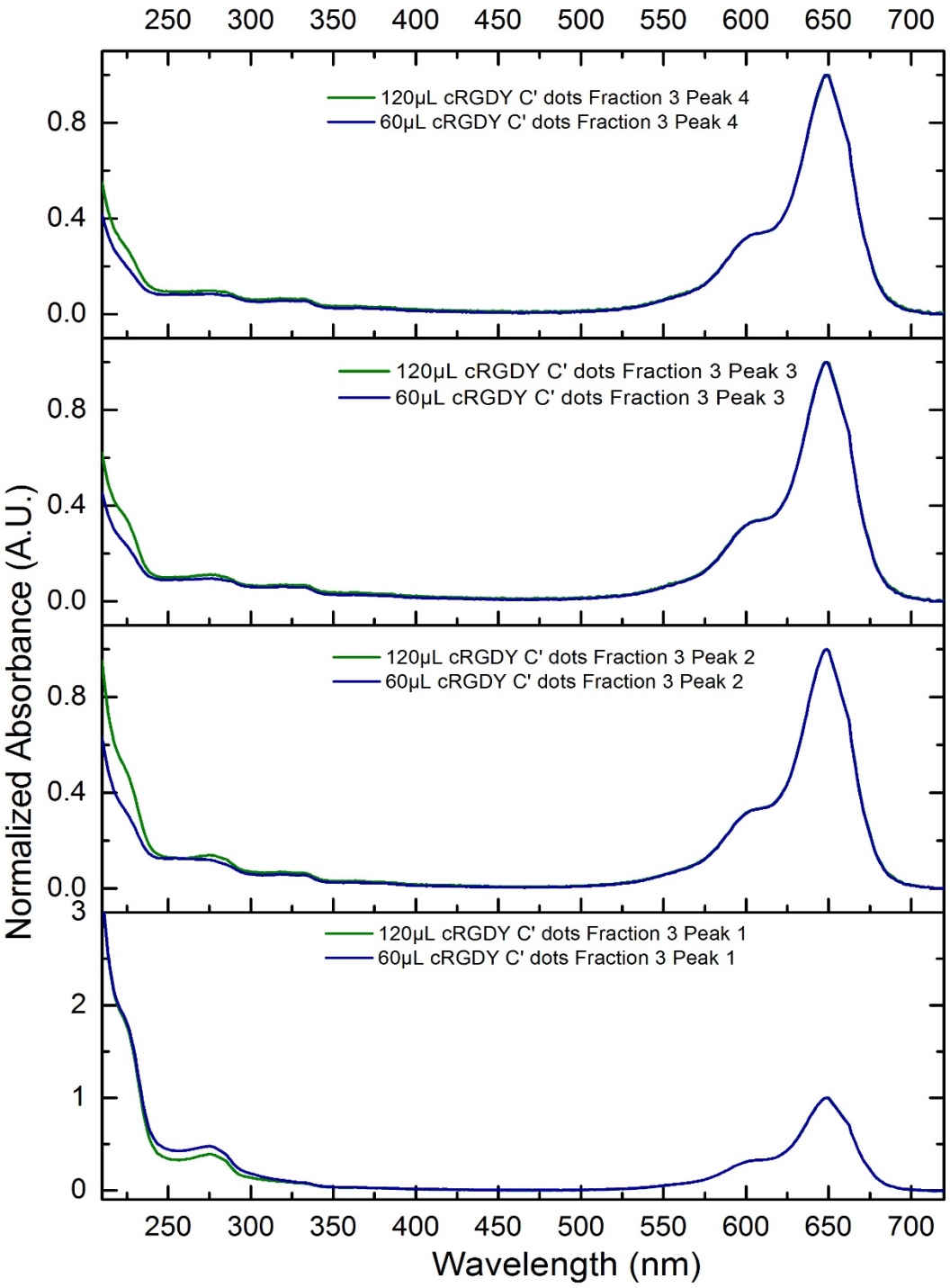

Figure 20: A stack plot of normalized absorbance spectra of HPLC chromatogram of fraction 3 peaks for 120 µL and 60 µL cRGDY C' dots GPC sorted by equivalent peak elution times for appropriate comparison.

Combined absorbance spectra of fractions and relative peak areas

Based on absorbance spectra of sample fractions, the observation is that relatively few particles contain a large amount of surface ligands while the majority of the particle population contains little to no ligands. Shown in Figure 21 where the absorbance at 275 nm was divided by the absorbance at 647 nm for each sample fraction peak to reveal this decreasing trend for increasing elution time. For further comparison, the absorbance spectra obtained for the different peaks of all fractions are combined in a single Figure 22. Absorbance spectra at the elusion time of 31 minutes (peak 1 for 120 µL cRGDY C' dot fractions 1, 2, 3, and 60 µL cRGDY C' dot fractions 2, 3, and peak 2 for fraction 1) across all fractions had a strong signal at 275 nm and shouldering at 225 nm. For peaks at later elution times, signals at 275 nm and shouldering at 225 nm decrease from moderate to little or no significant signal. However, from the 60 µL cRGDY C' dot fraction 3/ peak 3, a particularly strong signal and shouldering are visible. With the exception of fraction 3/ peak 3 from 60 µL cRGDY C' dots, features in the absorbance spectra appeared to be conserved across sample fractions and peaks. Similarities in absorbance spectra across all the sample fractions further support that distributions of surface ligands per particle are independent of particle size. However, the amounts of surface ligands per particle may increase or decrease based on particle size and quantifying these amounts is a subject of future research.

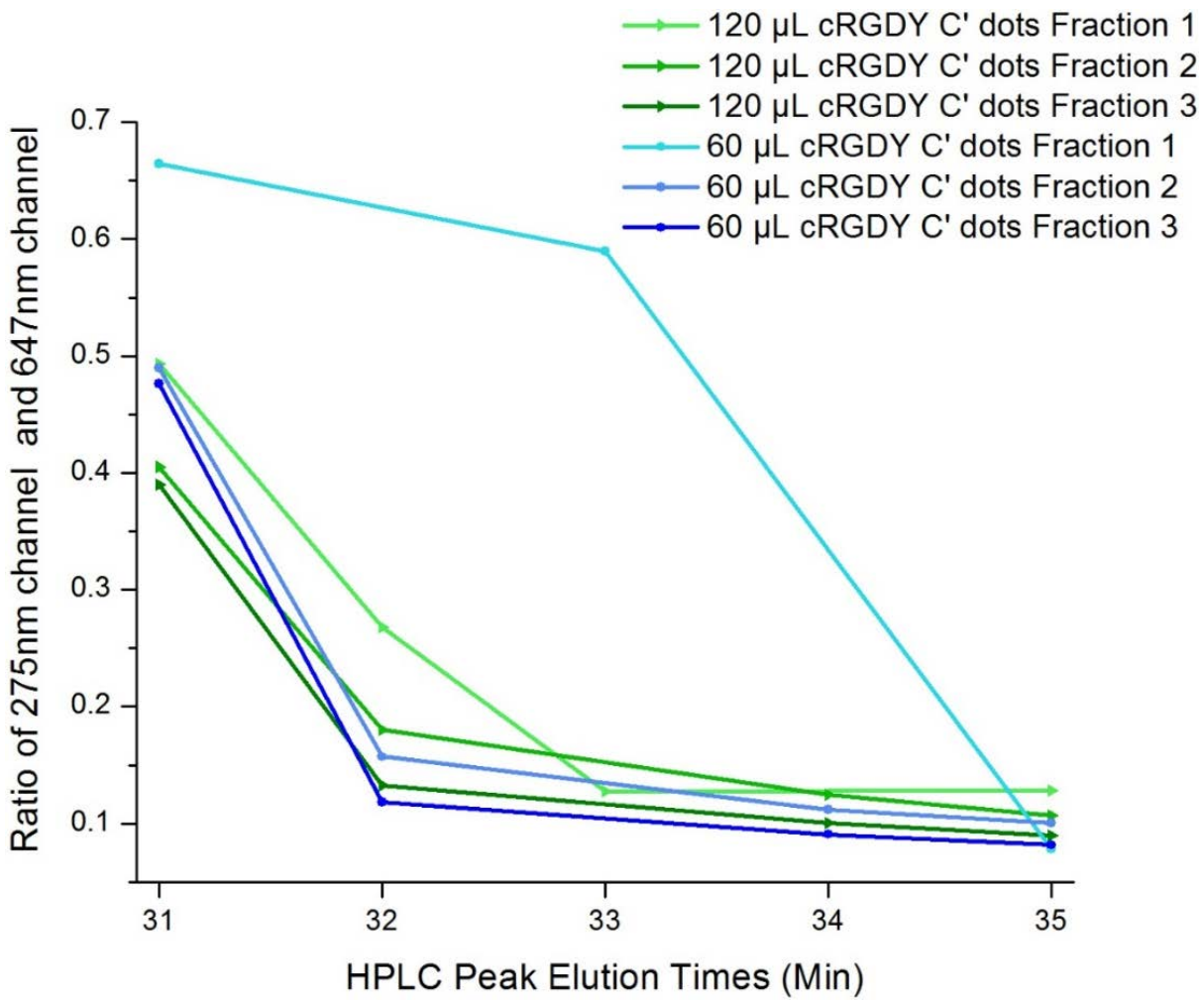

Figure 21: Absorbance spectra relation at 275 nm and 647 nm across each sample fraction with respect to HPLC peak elusion times

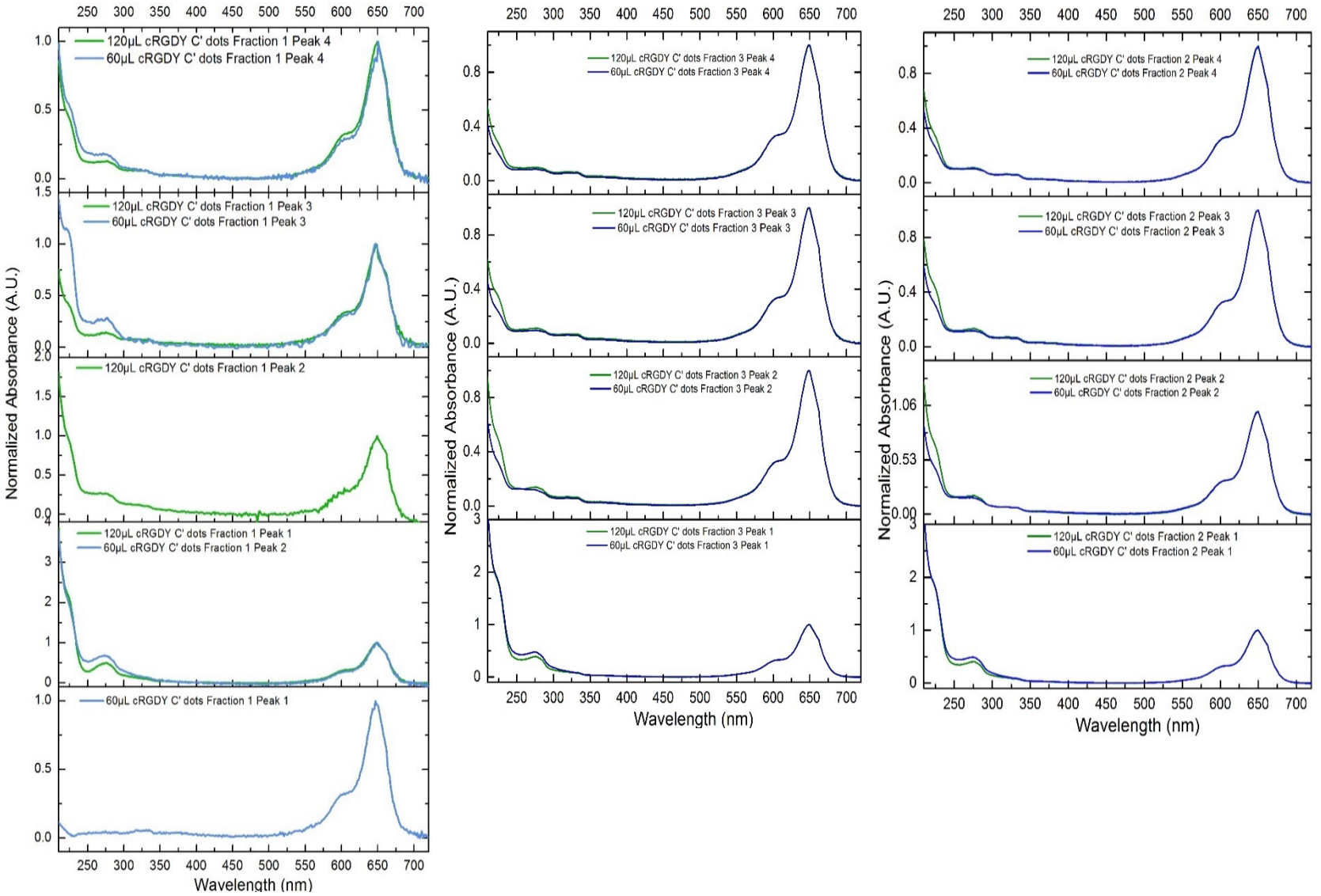

Figure 22: Combined stack plot of normalized absorbance spectrums of HPLC chromatogram peaks for 120 μL and 60 μL cRGDY C' dots GPC fractions 1(left), 2 (middle), and 3 (right) compared to corresponding peak elution times

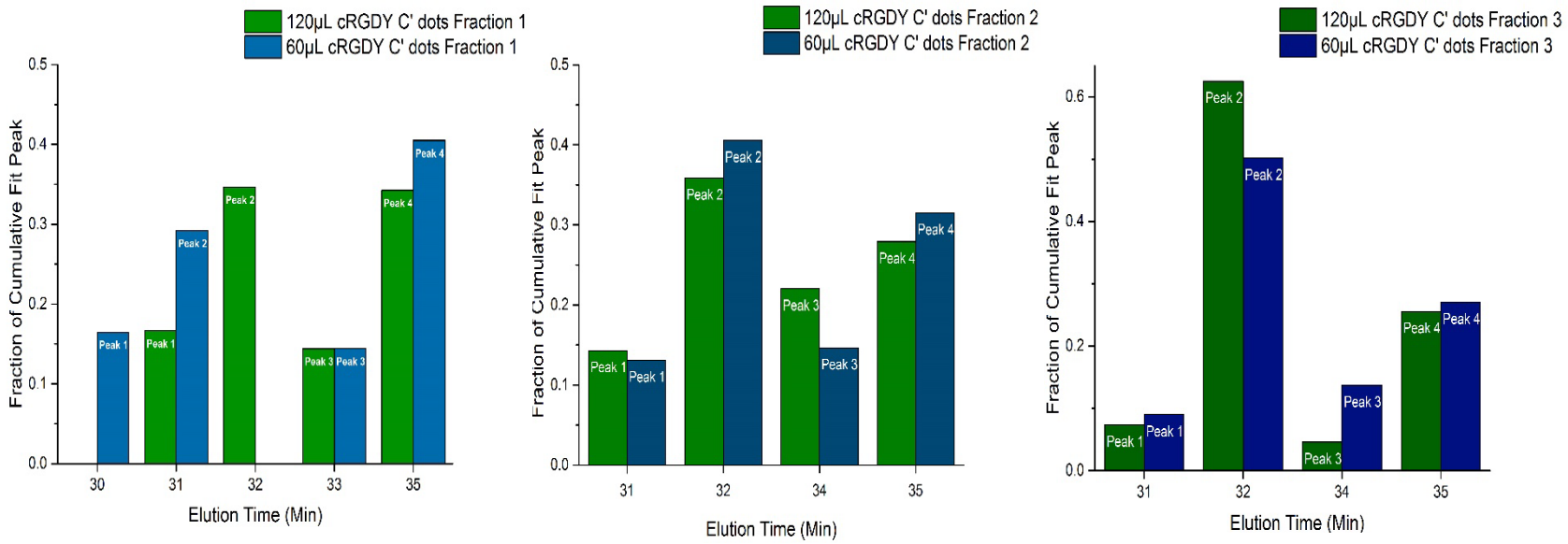

Figure 23: Relative area under each sample peak. (Left) Fraction 1; (Middle) Fraction 2; (Right) Fraction 3

Relative area under each fractionated sample peak as a function of peak elution time is shown in Figure 23 for the two different C' dot samples and fractions 1-3. Peak areas were divided by the respective cumulative fit peak areas from the modified Gaussian fit. Peaks at 32 and 35 minutes contain the majority of material while peaks at 31, 33, and 34 minutes had consistently less and similar amounts of material across samples and fractions. The relatively small amount of material at 31 minutes agrees with the postulation that very few particles contain a large amount of cRGDY. For fraction 1 in Figure 23 (left) amounts of material under each peak did not display clear patterns across sample fractions other than indicating that the distribution of relative amounts changes from fraction to fraction. Additionally, areas under each peak indicate the amount of material independent of the heterogeneity of the material present. Absorbance spectra for each peak from Figure 22 appear to be independent of relative peak amounts. Increases or decreases in relative areas across samples and fractions did not correlate with changes in peak heights at 275 nm or shouldering at 225 nm.

Un-fractionated 120 µL and 60 µL cRGDY C’ dot HPLC Chromatograms

A comparison of each un-fractionated sample to un-fractionated PEG C’ dots without cRGDY modification (Figure 24) shows similar peak features and elution times across all the chromatograms. These similarities indicate that PEG on the surface of the particles contributes significantly to particle separation and interactions with the column. Contributions from cRGDY distributions are apparent in the broadening of the peak when compared to a sample of only PEG C’ dots. From the absorbance spectra, and similarities in peak structure between PEGylated and cRGDY (with PEG) C’ dots, elucidating the exact contribution of cRGDY is more complex than initially postulated. The similarity in peak structure and elution times indicates that peak structure most likely originates from PEG distributions (e.g. PEG surface density, number of PEG per particle, and/or PEG binding conformation, brush versus mushroom), and not from cRGDY. This finding prompts further investigation with surface ligands with either a greater absorbance at 275 nm or a different absorbance wavelength entirely to differentiate contributions from PEG, Cy5, silica, and other constituents.

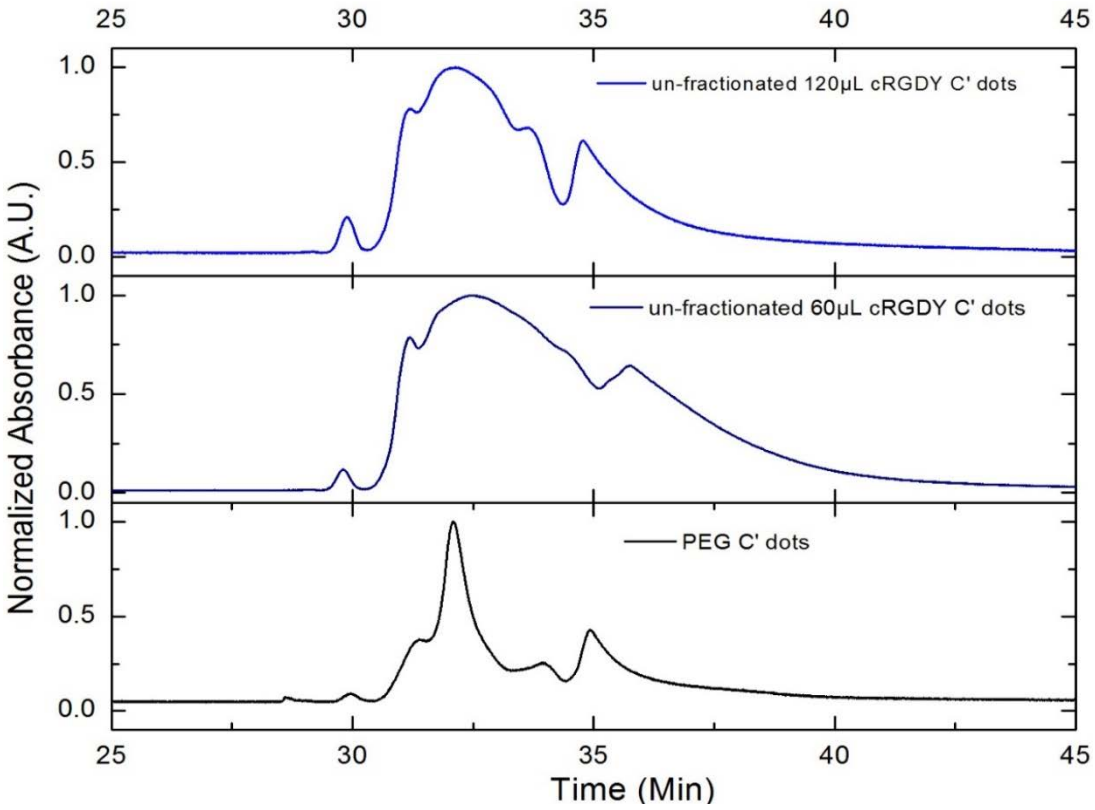

Figure 24: Stack normalized HPLC chromatograms of un-fractionated 120 µL and 60 µL cRGDY C' dots compared to un-fractionated PEG C' dots

CONCLUSIONS

The quantification of targeting ligand distributions on the surface of functionalized nanoparticles will enable researchers to elucidate the benefit of optimized architecture in theranostic applications. The results of this work provide a foundation for the study of surface ligand distributions of nanoparticles, and insight for the continued research and analysis of nanoparticles for their implementation in nanomedicine through analytical techniques not previously utilized.

Analytical discernment of the HPLC elugrams established the separation of C' dots based on physiochemical interactions between ligands on the particle surface, and the HPLC's column stationary phase with reasonable precision. HPLC chromatograms were modeled with a modified Gaussian distribution to yield a distribution of distributions with respect to surface ligands per particle. HPLC analysis revealed that cRGDY-PEG-C' dots systems may not be ideal due to the difficulty in elucidating cRGDY separation from PEG, when samples of un-fractioned cRGDY-PEG-C' dots were compared to chromatograms of PEG C' dots.

Results indicated particle size had little impact on surface ligand per particle distributions, shown by similarities of absorbance spectra under fractionated GPC HPLC chromatogram peaks for each sample. Additionally, observations of relative peak areas and absorbance spectra indicated that a small portion of the particle population contained large amounts of cRGDY while the majority of the population contained significantly less. Despite the inability to quantify exact cRGDY per particle distributions, the study demonstrated the existence of PEGylated particle distributions, which may influence the behavior of these materials for nanomedicine applications, more than previously thought.

FUTURE RESEARCH DIRECTIONS

As next steps, FCS measurements combined with optical spectroscopy may be performed on particles associated with each of the HPLC peaks obtained from different GPC fractions of PEG C' dots and cRGDY C' dots. This would provide specific numbers for e.g. hydrodynamic size, dyes per particles, and average number of cRGDY per particle for each of the individual HPLC peaks, thereby possibly elucidating the origin of these peaks. For example, based on observations by Ma *et. al.* it is possible that semi-encapsulated dyes may interfere with surface functionalization, since ~6nm-sized C' dots do not have a second silica shell, and may therefore not completely encapsulate dyes.[16] Besides better characterization of existing particle synthesis batches, an alternative direction may reside in the investigation of particle functionalization using microfluidics.

The use of microfluidics is now widespread in the fields of biotechnology and nanomedicine for drug design, delivery, detection and as diagnostic devices.[37] Such devices offer the ability to utilize micro structures to transport and manipulate fluids.[37] With microfluidics a larger parameter space may be explored for optimization in a rapid and systemic manner.[38] Nanoparticles may be synthesized in a microfluidic device continuously with improved control over ligand and dye placement.[39] As shown in Figure 25 microfluidics have been used for the continuous synthesis of Quantum Dots (Q Dots).[40] C' dots synthesized in a microfluidic device would be characterized with GPC, HPLC and FCS, with the expectation of increased particle homogeneity.

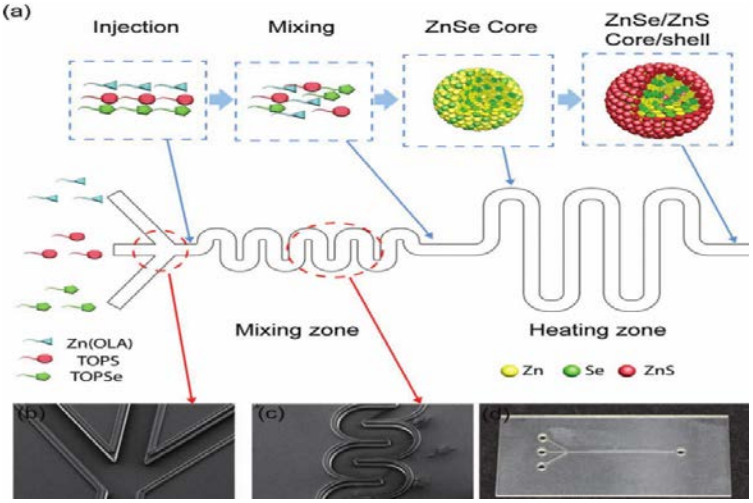

Figure 25: (a) Schematic of a microfluidic device used in the in situ synthesis of ZnSe/ZnS Core/shell Q Dots. (b, c) SEM images of: the injection and mixing zones (d) A photographic image of entire device.[40]

ACKNOWLEDGEMENTS

I would like to thank some of the people closest to me during my life and time at Cornell University, each of whom helped to comfort and support me. Most importantly, I must mention, my wife, Estefanía Alvarado, for her unyielding love, support, and compassion, which has not faltered through our difficulties, and for celebrating our accomplishments. My in-laws, Gledys and Carlos Hernandez, I appreciate them for their guidance, and parental love. My family, Manuel Negrete Polo, Margarita Luna Coavas, Yashua David Negrete “Lobo” Luna, and Samuel José Negrete Luna, who have treated me as their son and brother. Additionally, I would like to thank my close friend Melik Ziya Turker for his brotherly love, support, and laughs; and to Pat Comunale for his good wishes through snail-mail. In addition, I extend many thanks to my friends in the Wiesner Group: Ferdinand Kohle, Teresa Kao, Tom Gardinier, Sasha Andrievsky, Nikhil Dhawan, Tangi Aubert, Kasia Oleske, and Kai Ma, among many team members.

I am much obliged to the wonderful staff at Cornell that has reach into my path here, for your help, guidance, and company: Janna S. Lamey, Anitra M. Douglas-McCarthy, Sara X. Hernandez, Summer Garcia, and Penny Burke. I am also grateful to Barbi Jackson, Amanda Brown, Drs. Lewis Johns, Chang-Yu Wu, Paul Chadik, Yiider Tseng, and Ben Koopman from the University of Florida for their advice, friendship, and for helping me get to where I am now; I truly rest upon the shoulders of giants. Lastly, I am so very thankful for the opportunity to have been guided and advised by the most talented individuals I have ever had the pleasure of meeting: Linda Nowak, Abe Stroock, Fernando Escobedo, Matt DeLisa, Lynden Archer, Susan Daniel and my advisors, Harold Craighead and Uli Wiesner; thank you for advocating on my behalf and supporting me through this portion of my life.

REFERENCES

1. Ma, K., Zhang, D., Cong, Y. & Wiesner, U. Elucidating the Mechanism of Silica Nanoparticle PEGylation Processes Using Fluorescence Correlation Spectroscopies. *Chem. Mater.* **28,** 1537–1545 (2016).

2. Benezra, M. *et al.* Multimodal silica nanoparticles are effective cancer-targeted probes in a model of human melanoma. *J. Clin. Invest.* **121,** 2768–2780 (2011).

3. Xie, J., Lee, S. & Chen, X. Nanoparticle-based theranostic agents. doi:10.1016/j.addr.2010.07.009

4. Olivier, V. *et al.* Influence of Targeting Ligand Flexibility on Receptor Binding of Particulate Drug Delivery Systems. *Bioconjug. Chem.* **14,** 1203–1208 (2003).

5. Marre, S. & Jensen, K. F. Synthesis of micro and nanostructures in microfluidic systems. *Chem. Soc. Rev.* **39,** 1183–1202 (2010).

6. Mullen, D. G. *et al.* A quantitative assessment of nanoparticle-ligand distributions: Implications for targeted drug and imaging delivery in dendrimer conjugates. *ACS Nano* **4,** 657–670 (2010).

7. Mullen, D. G. & Banaszak Holl, M. M. Heterogeneous ligand-nanoparticle distributions: A major obstacle to scientific understanding and commercial translation. *Acc. Chem. Res.* **44,** 1135–1145 (2011).

8. Fakhari, A., Baoum, A., Siahaan, T. J., Le, K. B. & Berkland, C. Controlling ligand surface density optimizes nanoparticle binding to ICAM-1. *J. Pharm. Sci.* **100,** 1045–1056 (2011).

9. Ow, H. *et al.* Bright and stable core-shell fluorescent silica nanoparticles. *Nano Lett.* **5,** 113–117 (2005).

10. Wiesner, U., Ow, H., Larson, D. R. & Webb, W. W. Fluorescent silica-based nanoparticles: US 8298677 B2. 16 (2012).

11. Stöber, W., Fink, A. & Bohn, E. Controlled growth of monodisperse silica spheres in the micron size range. *J. Colloid Interface Sci.* **26,** 62–69 (1968).

12. Phillips, E. *et al.* Clinical translation of an ultrasmall inorganic optical-PET imaging nanoparticle probe. *Sci. Transl. Med.* **6,** 260ra149 (2014).

13. Burns, A. A. *et al.* Fluorescent silica nanoparticles with efficient urinary excretion for nanomedicine. *Nano Lett.* **9,** 442–448 (2009).

14. Choi, C. H. J., Zuckerman, J. E., Webster, P. & Davis, M. E. Targeting kidney mesangium by nanoparticles of defined size. *Proc. Natl. Acad. Sci. U. S. A.* **108,** 6656–61 (2011).

15. Kim, S. E. *et al.* Ultrasmall nanoparticles induce ferroptosis in nutrient-deprived cancer cells and suppress tumour growth. (2016). doi:10.1038/NNANO.2016.164

16. Ma, K. *et al.* Control of Ultrasmall Sub-10 nm Ligand-Functionalized Fluorescent Core-Shell Silica Nanoparticle Growth in Water. *Chem. Mater.* **27,** 4119–4133 (2015).

17. Bradbury, M. S. *et al.* Clinically-translated silica nanoparticles as dual-modality cancer-targeted probes for image-guided surgery and interventions. *Integr. Biol. (Camb).* **5,** 74–86 (2013).

18. Harris, J. M. & Chess, R. B. Effect of pegylation on pharmaceuticals. *Nat. Rev. Drug Discov.* **2,** 214–221 (2003).

19. *Oxford Dictionary of Biochemistry and Molecular Biology*. (Oxford University Press, 2006).

20. Herz, E. Synthesis, Characterization, and Optical Properties of Colloidal Organic Dye-Containing Fluorescent Core-Shell Silica Nanoparticles. *Dissertation* (2009).

21. Thompson, N. L. & Mitchell, J. L. 21 High Order Autocorrelation in Fluorescence Correlation Spectroscopy. (2001).

22. Larson, D. R. *et al.* Silica nanoparticle architecture determines radiative properties of encapsulated fluorophores. *Chem. Mater.* **20,** 2677–2684 (2008).

23. Schwille, P., Kummer, S., Heikal, A. A., Moerner, W. E. & Webb, W. W. Fluorescence correlation spectroscopy reveals fast optical excitation-driven intramolecular dynamics of yellow fluorescent proteins. *Proc. Natl. Acad. Sci. U. S. A.* **97,** 151–6 (2000).

24. Cussler, E. L. *Diffusion: Mass Transfer in Fluid Systems*. *Engineering* **Second,** (1997).

25. Elson, E. L. Fluorescence correlation spectroscopy: Past, present, future. *Biophys. J.* **101,** 2855–2870 (2011).

26. Einholm, E. J. Introduction to Spectroscopy. *J. Magn. Reson. A* **121,** 93–94 (1996).

27. Sommer, L. *CHAPTER 1 - Basis of Spectrophotometry in the Uv and Vis Regions*. *Analytical Absorption Spectrophotometry in the Visible and UltravioletThe Principles* **Volume 8,** (Elsevier Science Ltd, 1989).

28. Snyder, L. R., Kirkland, J. J. & Dolan, J. W. *Basic Concepts and the Control of Separation*. *Introduction to Modern Liquid Chromatography* (John Wiley & Sons, Inc., 2010). doi:10.1002/9780470508183.ch2

29. Pasch, H. & Trathnigg, B. *Multidimensional HPLC of Polymers Springer Laboratory Manuals in Polymer Science*. (Springer, 2013).

30. Scientific, L.-G. C. The Theory of HPLC. Chromatographic Parameters. *E-learning Anal. Chem. Community* **2014,** (2014).

31. Ng, L. L. *Center for Drug Evaluation and Research (CDER) Reviewer Guidance' Validation of Chromatographic Methods*. (1994).

32. Grushka, E. Characterization of Exponentially Modified Gaussian Peaks in Chromatography. *J. Anal. Chem.* **44,** 1734–1738 (1972).

33. Mullen, D. G. *et al.* The implications of stochastic synthesis for the conjugation of functional groups to nanoparticles. *Bioconjug. Chem.* **19,** 1748–1752 (2008).

34. Woll, D. Fluorescence correlation spectroscopy in polymer science. *Rsc Adv.* **4,** 2447–2465 (2014).

35. Zhegalova, N. G., He, S., Zhou, H., Kim, D. M. & Berezin, M. Y. Minimization of self-quenching fluorescence on dyes conjugated to biomolecules with multiple labeling sites via asymmetrically charged NIR fluorophores. *Contrast Media Mol. Imaging* **9,** 355–362 (2014).

36. Barazzouk, S. & Daneault, C. Amino Acid and Peptide Immobilization on Oxidized Nanocellulose: Spectroscopic Characterization. *Nanomaterials* **2,** 187–205 (2012).

37. Zimmerman, W. *Microfluidics: history, theory and applications*. (Springer, 2006). doi:978-1-62100-034-1

38. Voicu, D. *et al.* Kinetics of multicomponent polymerization reaction studied in a microfluidic format. *Macromolecules* **45,** 4469–4475 (2012).

39. Hung, L.-H. Micro/Nanoparticle Synthesis by Microfluidic Devices for Biomedical Applications. (University of California Irvine, 2007).

40. Kwon, B. H. *et al.* Continuous in situ synthesis of ZnSe/ZnS core/shell quantum dots in a microfluidic reaction system and its application for light-emitting diodes. *Small* **8,** 3257–3262 (2012).